ABSTRACT

Title of Document: IMPACT OF BOARD PAD FINISH ON THE SNPB AND LEAD-FREE SOLDER INTERCONNECT RELIABILITY FOR LEADLESS CHIP RESISTORS UNDER RANDOM VIBRATION LOADING

Gustavo Plaza, Master of Science, 2008

Directed By: Professor Michael Pecht
Department of Mechanical Engineering

The results from a step-stress random vibration tests are used to assess the interconnect reliability of various solder, component terminal and printed wiring board pad finishes. The durability assessment of leadless chip resistors attached with tin-lead and tin-silver-copper is examined. Component terminal finish, tin and tin-lead, in tin-lead soldered assemblies are examined. The board pad finishes used in the assemblies tested included immersion tin, immersion silver, electroless or electrolytic nickel immersed in gold, and organic solderability preservative, while tin-lead hot air solder leveling pad finish assembled with tin-lead solder served as a baseline. Destructive failure analysis is used to assess failure locations. Although the results obtained from the test indicate that under the vibration regimen studied no

significant difference was found between the durability of tin-lead and tin-silver-copper assemblies, the lead-free components did outperform the tin-lead assemblies. Pad finish is found to have a greater influence on tin-lead as compared to tin-silver-copper soldered assemblies. Immersion silver and electroless or electrolytic nickel immersed in gold showed the best durability results.

Impact of Board Pad Finish on the SnPb and Lead-free Solder Interconnect Reliability for Leadless Chip Resistors under Random Vibration Loading

By

Gustavo Alberto Plaza

Thesis submitted to the Faculty of the Graduate School of the
University of Maryland, College Park, in partial fulfillment
of the requirements for the degree of
Master of Science
2008

Advisory Committee:
Professor Michael Pecht, Chair
Professor Abhijit Dasgupta
Professor Donald Barker
Dr. Michael Osterman

Dedication

To my parents, Rafael and Ines.

Acknowledgements

I want to express my appreciation to Professor Michael Pecht, my thesis advisor, for all his support and guidance. I would also like to specially thank Dr. Michael Osterman for his constant guidance and patience throughout my work at CALCE.

I would like to thank the members of the thesis committee, Professor Donald Barker and Professor Abhijit Dasgupta, for their advice and support during my research and courses work. I would also like to thank, Dr. Michael Azarian, Dr. Diganta Das and Dr. Moustafa Al-Bassyiouni for their kindness, support and guidance in different stages of my thesis.

In addition, I want to acknowledge the students and staff at CALCE, who have been supportive throughout.

Finally, the most special appreciation goes to my parents, family and friends who have loved me and supported me throughout this special journey.

Table of Contents

List of Tables

List of Figures

Chapter 1: Introduction

1.1 Problem Statement

In the transition toward lead-free electronics, different board pad finish systems have emerged as alternatives to the assembly providers and manufacturers. Alternatives include immersion silver, immersion tin, electroless nickel-immersion gold, and organic solderability preservative. These board pad finishes provide temporary protection from surface oxidation and corrosion which may degrade solderability. Upon assembly, the board pad finish is consumed allowing the solder to create a strong electrical and mechanical bond.

Vibration environments are encountered in the useful life of electronic components and equipments under different applications such as commercial vehicles, military, avionic and even well drilling tools [1]. Under these environments, the solder interconnect reliability may be influenced by the solderable interface created by the deposition of board pad finishes prior to the application of the solder paste in the assembly process. Therefore, the impact of board pad finish on the reliability of solder interconnect under random vibration needs to be understood.

1.2 Background and Literature Review

Literature shows that different methods and approaches are used to measure the fatigue life of interconnects when exposed to true field environments. Random vibration fatigue

loading of the solder joint has been calculated using board strain through finite element analysis (FEA) modeling. Studies [2][3][4] were able to incorporate this methodology to predict failure time. Wong et al. [5] showed that the board strain can be used as a metric to study solder joint fatigue due to their linear relationship as obtain through FEA. Zhou et al. [6] used the board strain to measure the strain transfer function for both tin-silver-copper and tin-lead solder using FEA.

Miner's rule has also been widely used to estimate the damage accumulated through different stress or strain levels. Qi [7] used the methodology proposed by Barker et al. in 1990 to develop an integrated rapid solder joint fatigue life-prediction simulation approach for ball grid array (BGA) components under a combined vibration and thermal cycling loading. Gu et al. [8] used it to predict the life consumed of an electronic component and calculate remaining life. Chen et al. [4] used Miner's rule in combination with a derived S-N curve from their test data to predict remaining life of components exposed to random vibration for validation purposes.

A fundamental vibration fatigue model proposed by Basquin in 1910 [9] has also been widely used to represent failure by a straight line on a log-log plot of stress range versus cycles to failure. An empirical solution derived by Steinberg [10] from Basquin's model is one of the most widely known applications of this model. The model assumes proportionality between stress range and reversing out-of-plane displacement to estimate the life of a component interconnects under a known of the loading magnitude. The latest

iteration of this model includes printed wiring board (PWB) characteristics, random vibration level, natural frequency and a factor to consider the component package type.

Vibration durability studies [5][6][12][13][14] have been conducted using tin-lead solder as this was the most widely used material in the industry. A few characterization and reliability studies under vibration environments have been performed using lead-free materials especially tin-silver-copper. Wong *et al.* [5] compared the strain-life curves of SnPb versus SnAgCu and found that the lead-free system has a better high-cycle fatigue performance. Woodrow [12][13] found vibration fatigue life was a function of position, part type and solder material. In some cases, components soldered with SnPb were found to be more reliable than Pb-free soldered assemblies while in other cases Pb-free (SAC) solder interconnects survived longer. Lee *et al.* [14] used PBGA assemblies to compare the reliability of lead-free assemblies versus eutectic SnPb under random vibration and thermal cycling. In that study, Lee found that Pb-free solder interconnects have a much longer thermal fatigue life than Sn37Pb while no significant difference was found between these assemblies under random vibration loading as no failures were found. Further, the motivation of this work is based on the lack of studies focusing on the impact of the board pad finish materials on solder interconnect durability exposed to random vibration conditions.

Copper is the most widely used metallization material for PWBs. But due to its fast oxidation when exposed to the environment, different finish systems are used to protect the copper and preserve solderability in electronic applications. Since the industry has

transitioned toward the Pb-free, the popular Pb-based hot air solder leveling has been replaced by lead-free systems which include immersion tin (ImSn), immersion silver (ImAg), electroless or electrolytic nickel under immersion gold (ENIG), and organic solderability preservative (OSP) [16]. These board pad finish systems may influence the interfacial intermetallics fatigue failures due to brittleness and excessive growth of intermetallic compounds (IMCs) which may degrade the reliability of solder joints [17]. Spowage *et al.* [18] found that ImAg and ImSn had comparable IMC growths while ENIG showed the smallest IMC growth and OSP showed the highest. Studies [19][20][21][22][23] reported some reliability issues associated with these lead-free board pad finishes. Although ENIG has a long shelf life time due to the gold layer that protects the nickel from oxidation, Zeng *et al.* [19] and Goyal et al. [20] reported reliability concerns as they found the possibility of gold embrittlement which may weakness the interconnect and failures at the interface between the nickel layer and the IMC, respectively. Fang *et al.* [21] reported early fatigue failures of solder joints attached onto an OSP board pad finish when exposed to thermal shock cycling. In case of the ImAg, corrosion in the silver layer has been found when exposed to the atmosphere both during storage and under operating conditions [22]. Houghton [23] has also studied the influence of board pad finish on the solder joint strength finding that ImAg had the highest lead pull strengths when compared to ENIG and ImSn.

1.3 Overview of Thesis

This work presents the results used to assess the durability of Sn37Pb (SnPb) and Sn3.0Ag0.5Cu (SAC) surface mount technology (SMT) solder joints under random

vibration loading conditions. Strain measurements collected during the vibration test are used to map the response of the printed wired board (PWB) in FEA under different excitation conditions. In addition, failure analysis is conducted to verify the mechanisms and locations of electrical discontinuities. The random vibration fatigue model developed by Steinberg [10] is used to adjust the time-to-failure (TTF) to a common load level. Analysis of variance (ANOVA) on the adjusted TTF data is performed to evaluate the influence of the board pad finish on the solder interconnect reliability of the leadless chip resistors (LCRs). Finally, the random vibration reliability of SnPb soldered interconnects is compared with mixed and SAC soldered interconnects assembled with different board pad finishes using weibull plots.

Chapter 2: Vibration Test

Random vibration accelerated fatigue damage applied to the surface mount solder interconnects is investigated experimentally. Section 2.1 outlines the design and characterization of a test vehicle and a test fixture. Section 2.2 outlines the loading profile and test characteristics. In section 2.3, the failure criteria used to define failure time is discussed.

2.1 Test Vehicle and Fixture

Vibration test was developed and conducted on a common test vehicle design. The vehicle and fixture are discussed in the following sections.

2.1.1. Test Vehicle

Experimental test data was generated using test vehicles of common design. A sample test assembly is presented in Figure 1. The design included positions for 1mm pitch 256-IO ball grid arrays (BGAs), 0.8 mm pitch 100-IO quad-flat packages (QFPs) and leadless chip resistors (LCR) of two sizes to be mounted on a PWB constructed with two copper layers. The overall dimensions of the boards were 177.8 mm x 203.2 mm and a thickness of 1.64 mm. The FR-4 board material was characterized previously by Qi et al. [24]. Measured properties included a glass transition temperature (Tg) of 180ºC, in-plane CTE 14ppm/ºC, elastic modulus at 25 ºC of 23,982 MPa below the Tg, and the elastic modulus above the Tg at 200ºC of 5,776 MPa. Table 1 shows the number of components that were assembled to each of the test board and the daisy chained nets available for continuous electrical resistance monitoring.

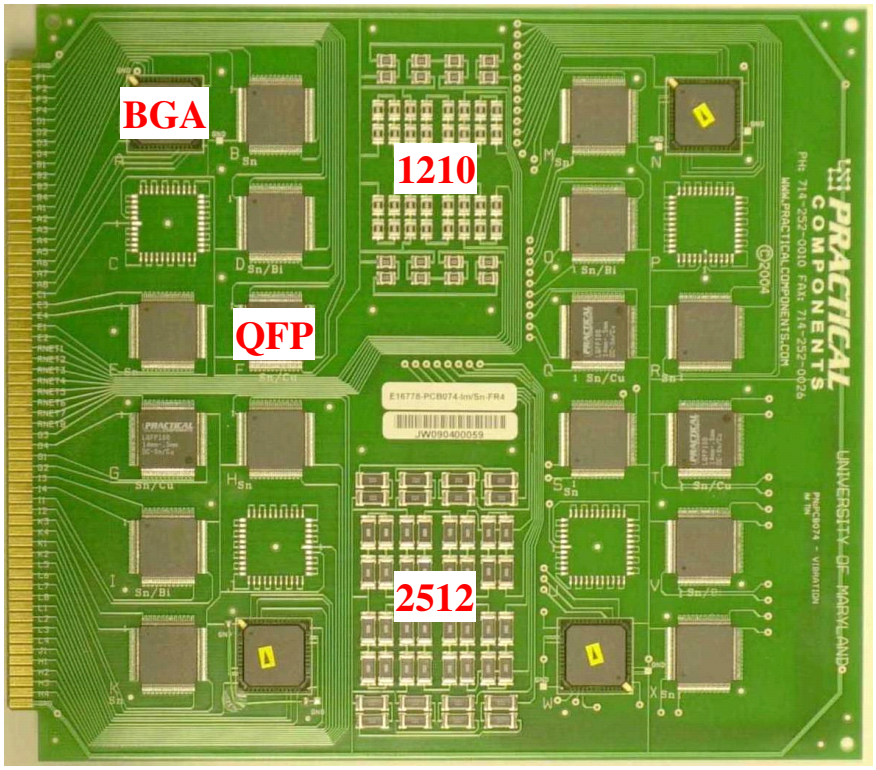

Figure 1 – Test Vehicle

Table 1 – Test Vehicle

Name	Number of Components	Number of Daisy Chains
BGA (256 balls)	4	8 per BGA
QFP (100 leads)	16	4 per QFP
1210 LCR	48	8
2512 LCR	48	8

Component termination, solder and board pad finish material combinations were created and tested. Test boards with SnPb terminal parts assembled with Sn37Pb solder paste onto a SnPb hot air solder leveling (HASL) finish served as baseline. Pb-free assemblies used lead-free (Sn, SnBi, SnCu, SnAgCu) terminal parts assembled with Sn3Ag0.5Cu solder paste and lead-free board pad finishes. The mixed assemblies were made with

Sn37Pb solder paste, lead-free (Sn, SnBi, SnCu, SnAgCu) terminal components and lead-free and HASL board pad finishes. The board termination systems used included HASL for the SnPb assembly, InSm, ImAg, ENIG and OSP for the Pb-free assemblies and all five systems for the mixed solder assembly. All assemblies were aged at a constant temperature of 125ºC for a period of 100 hours prior to the random vibration durability test. The durability test matrix is summarized in Table 2 including the number of boards tested for each of the board pad finishes.

Table 2 – Assembly Matrix

Identifiers	Solder ball or lead finish	Solder paste	Board Pad finish	# of Boards
SnPb	Sn37Pb ball – BGA Sn37Pb finish – QFP, Resistors	Sn37Pb	HASL	2
Pb-free	Sn3.0Ag0.5Cu ball – BGA Sn, Sn0.7Cu, Sn2.0Bi finish – QFP Sn finish – Resistors	Sn3.0Ag0.5Cu	ImSn	2
			ImAg	2
			ENIG	2
			OSP	2
Mixed	Sn3.0Ag0.5Cu ball – BGA Sn, Sn0.7Cu, Sn2.0Bi finish – QFP Sn finish – Resistors	Sn3.0Ag0.5Cu	HASL	2
			ImSn	2
			ImAg	2
			ENIG	2
			OSP	2

2.1.2. Test Fixture

The test cards were loaded into the fixture shown in Figure 2. This fixture was designed to hold up to 20 test assemblies for the vibration durability test. The fixture was attached to an electro-dynamic vibration system with the reversed vibration motion normal to the flat surface of the test assembly (out-of-plane displacement). Assemblies were secured to the test fixture using two fiber glass clamps that held the test assemblies along the short edges (Figure 1).

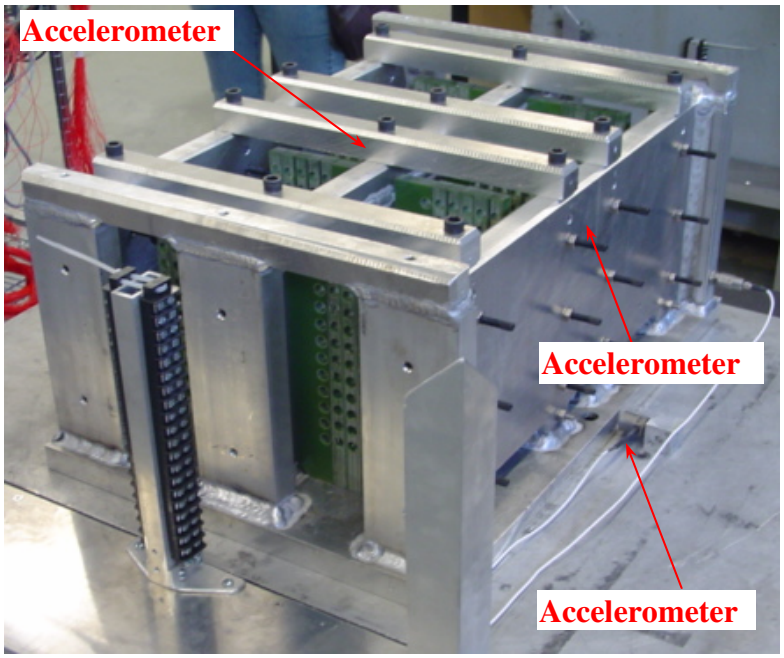

Figure 2 – Test Fixture

2.1.3. Test Fixture Characterization

A characterization test was performed prior to the durability test to measure the fixture's response to a vibration environment. Accelerometers were attached at different locations of the fixture as depicted in Figure 2. After adding aluminum cross bars, which are not shown in Figure 2, to increase the stiffness of the fixture, a first natural frequency of

approximately 750 Hz was achieved. The sine sweep response from 50 Hz to 1000 Hz of the fixture is shown in Figure 3. Previously performed random vibration simulations of the test vehicle had shown the first mode frequency of an individual test assembly to be approximately 200 Hz. Therefore, interaction between the test boards and the test fixture was assumed to be negligible.

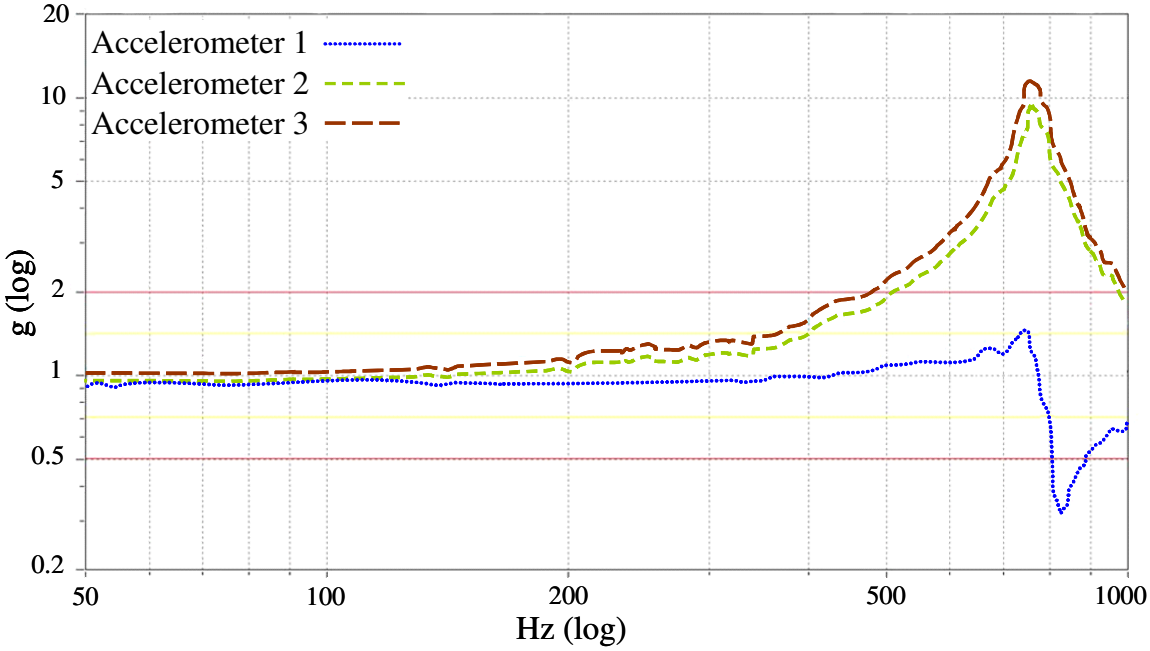

Figure 3 – Fixture Characterization Response

2.1.4. Test Vehicle Chracterization

The board responses were also characterized prior to the durability test. Eight strain gages were attached to the back of the PWBs as shown in Figure 4. The characterization test was performed at six different excitation levels that range from 0.02 G^2/Hz to 0.2 G^2/Hz and a frequency range from 10 Hz to 500 Hz, with a 4dB/octave roll-off on both sides. Micro-strain measurements were collected using data loggers that were able to sample up to 2,000 data points per second. The strain measurements were used to

calculate the frequency response of the PWB using Fast Fourier Transform and calibrate a simulation model of the board in FEA.

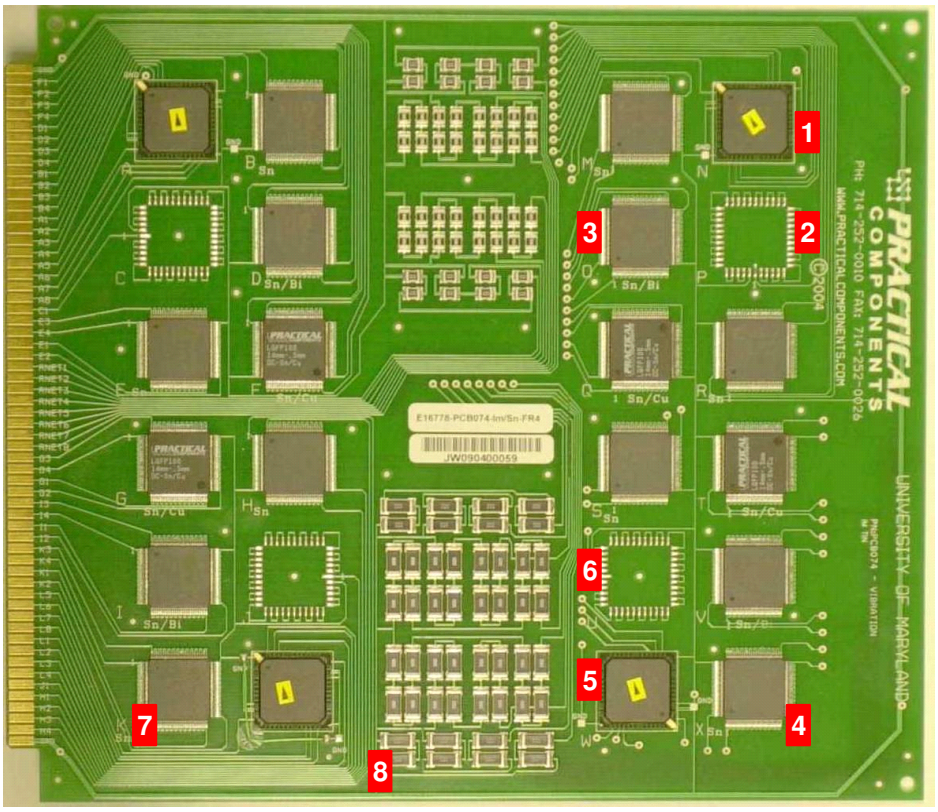

Figure 4 – Strain Gage Locations for Characterization Test.

2.2 *Test Characteristics*

A random vibration step stress profile, shown in Figure 5, was applied on sets of mounted test assemblies to assess assembly reliability. Four random vibration levels from 0.02 G^2/Hz to 0.2 G^2/Hz over a frequency range from 10Hz to 500 Hz were used. On the first three random vibration levels, the excitation magnitude was held constant for six hours while the highest excitation level was applied for eighteen hours in periods of six hours each. Table 3 provides a summary of the stress profile used in the study.

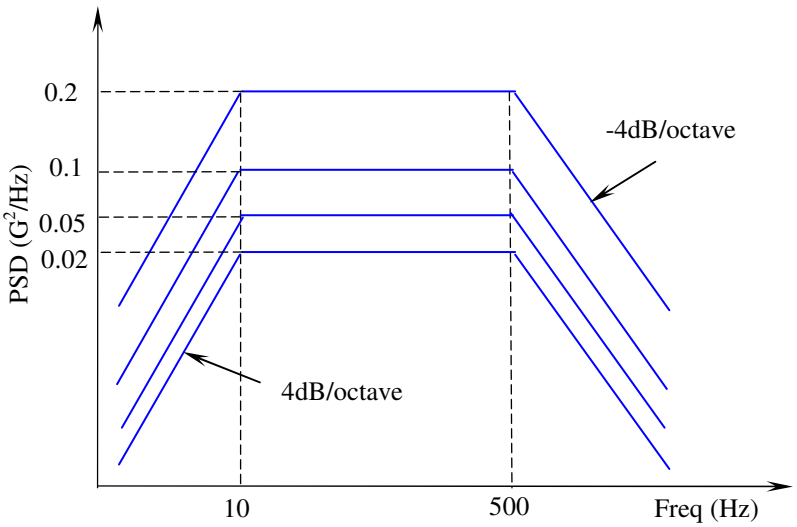

Figure 5 – Power Spectral Density Input Curve

Table 3 – Step-Stress Profile

PSD level (G²/Hz)	0.02	0.05	0.1	0.2
Time (hours)	6	6	6	18
Total Grms (in./sec²)	4.13	5.96	8.02	10.94

2.3 Failure Definition

To monitor the health of the surface mount interconnects during the random vibration tests, Agilent data loggers continuously measured the electrical resistance across each daisy chain net. The instrument records data over time at a sampling rate which is limited by its capabilities. This stored data is further used to analyze the failure time of a component after completion of the test.

Standards available to the industry and academia to define the failure based on resistance data acquired during the test suggest different conditions of failure. For example, IPC-

785 (Guidelines for Accelerated Reliability Testing of Surface Mount Solder Interconnects) [25] defines failure time on the first interruption of electrical continuity above 300 ohms followed by 9 consecutive interruptions within an additional 10% of the elapsed time. However, the instrument recommended for this definition is an event detector which is able to continuously monitor the electrical continuity of a net. Standard IPC-9701 (Performance Test Methods and Qualification Requirements for Surface Mount Solder Attachments) [26] defines failure, in case a data logger is used, as a 20% increase or higher of the nominal resistance in 5 consecutive readings.

These standards, along with another failure criteria that is further explained, were evaluated in this study prior to selecting the criterion used to define interconnect failures. IPC-9701 and IPC-785 are identified in Table 4 as C1 and C3, respectively. C2 is the other criterion evaluated which define failure as an increase in the resistance above a hard threshold of 25 ohms followed by 9 consecutive interruptions within an additional 10% of the elapsed time. Table 4 is an example of the comparison of the failure time identified by each of these criteria. As it can be observed in this table, IPC-9701 found all failures prior to the other criterion evaluated, therefore, it was chosen to be the most suitable to study the failure time of the components tested under the random vibration test.

Table 4 – Failure Criteria Evaluation

		Failure Criteria (min)		
Component		**C1**	**C2**	**C3**
QFP-G-Cu	G4	498	601	729
QFP-K	K4	773	774	780
QFP-G-Cu	G2	781	792	1135
2512	R1NET2	887	905	-
BGA-A	A5	887	905	1100
BGA-A	A4	948	995	1114
QFP-E	E4	1081	1082	1086
QFP-K	K3	1093	1096	1123
BGA-A	A8	1094	1102	1123
QFP-I-Bi	I4	1104	1112	1169
BGA-N	N8	1116	1119	1203
BGA-N	N5	1180	1202	1299
2512	R1NET1	1254	1272	-
BGA-L	L4	1321	1386	1860
BGA-N	N4	1413	1440	1477
QFP-R	R4	1417	1437	1497
QFP-I-Bi	I2	1367	1571	-
BGA-A	A1	1440	1440	1440
1210	RNET7	1530	1531	1583
QFP-I-Bi	I1	1540	1554	-
BGA-L	L6	1555	1557	1681
1210	RNET2	1687	1695	1782
BGA-L	L1	1687	1912	-
BGA-N	N3	1882	1883	-
QFP-G-Cu	G1	1912	1914	1939
QFP-E	E3	1921	1939	-
1210	RNET8	1921	2108	-

A failure signature from the test is depicted in Figure 6. The resistance of the daisy chain had remained stable at approximately 1.4 ohms during the initial 18 hours of testing. Just before 30 minutes under the 0.2G²/Hz excitation level, the health of the interconnect started to degrade until the circuit fully opened for the rest of the test.

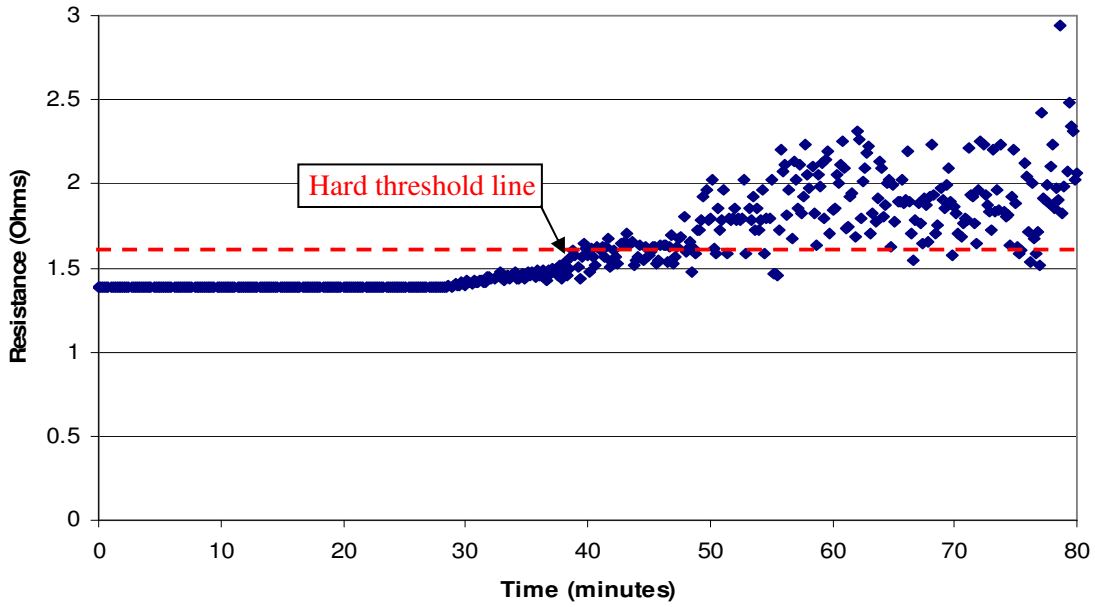

Figure 6 - Example of Failure Signature

Chapter 3: Test Results

Failure analysis and test results are discussed in this chapter. Section 3.1 discusses the results obtained from a destructive failure analysis and an examination performed through the use of Environmental Scanning Electron Microscope. Section 3.2 discusses the results obtained from the durability test. Section 3.3 discusses an approach taken to adjust the time-to-failure obtained in the durability test to a common load level. This approach is implemented and discussed in section 3.4.

3.1 Failure Analysis

After the vibration durability test, a destructive failure analysis was conducted to identify failure sites and mechanisms. For the purpose of this work, the 2512 LCRs will be the focus of the discussion. The failure analysis was conducted by electrical probe, cross-sectioning the components of interest and examination of potential failure sites under optical and Environmental Scanning Electron Microscope (E-SEM).

Figure 8 through Figure 13 show micro-sections of failed SnPb, mixed and lead-free interconnects. As illustrated in Figure 7, the cross-sectioned of all SnPb, mixed and lead-free assemblies show cracks that propagate from the toe of the solder fillet and through the interface between the intermetallics and the bulk of the solder. On the SnPb assemblies, as the crack propagated toward the component, it switched its path and continued propagating through the interface between the component and into the metallization of the end termination as shown in Figure 8. This was not observed with the components with Sn finished terminals. For the SnPb assemblies, the SnPb finished

terminals of the LCR parts were larger compared to the Sn finished terminals. The size on the SnPb finished terminal may play a role in crack path formation. Figure 11 shows an example of the crack initiation point in the fillet of the solder joint which is consistent for all assemblies. Blattau *et al.* [27] also found this to be the crack initiation point through failure analysis and FEA on components subjected to non-reversed high-cyclic bending test.

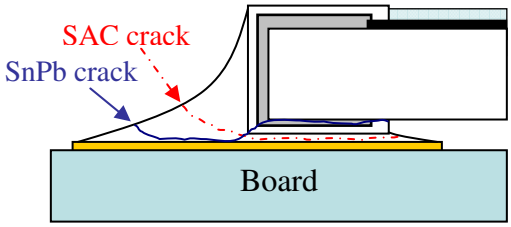

Figure 7 – Crack Propagation Difference for SnPb and SAC LCRs

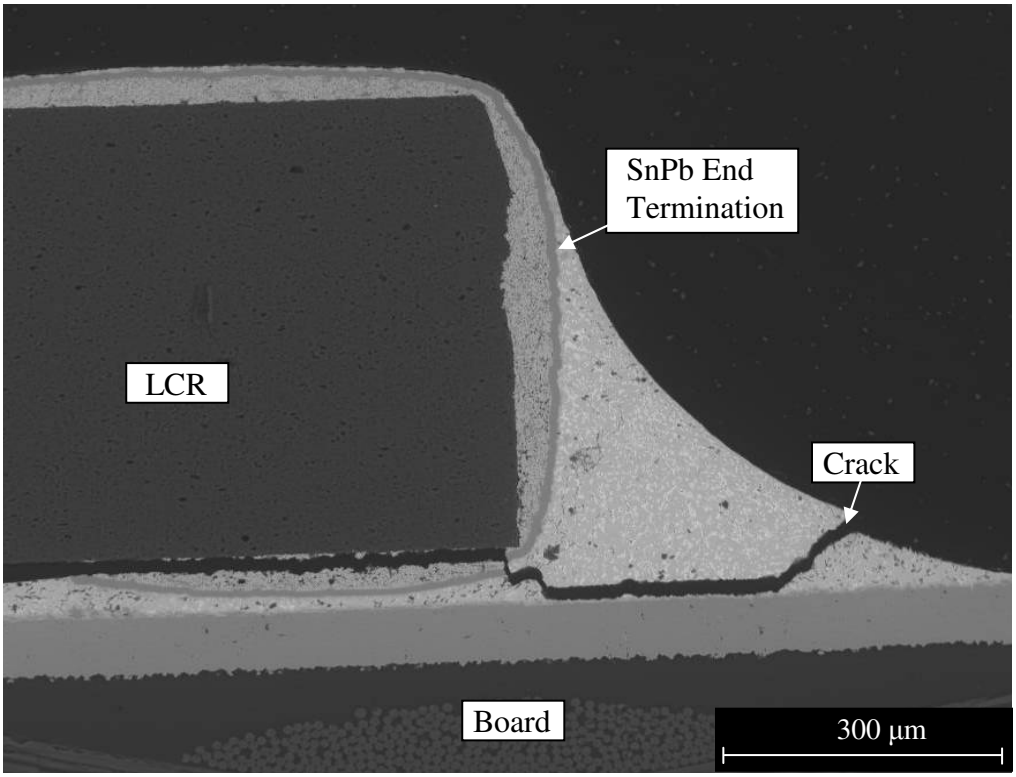

Figure 8 - SnPb-HASL after Aging at 125ºC for 100 hrs

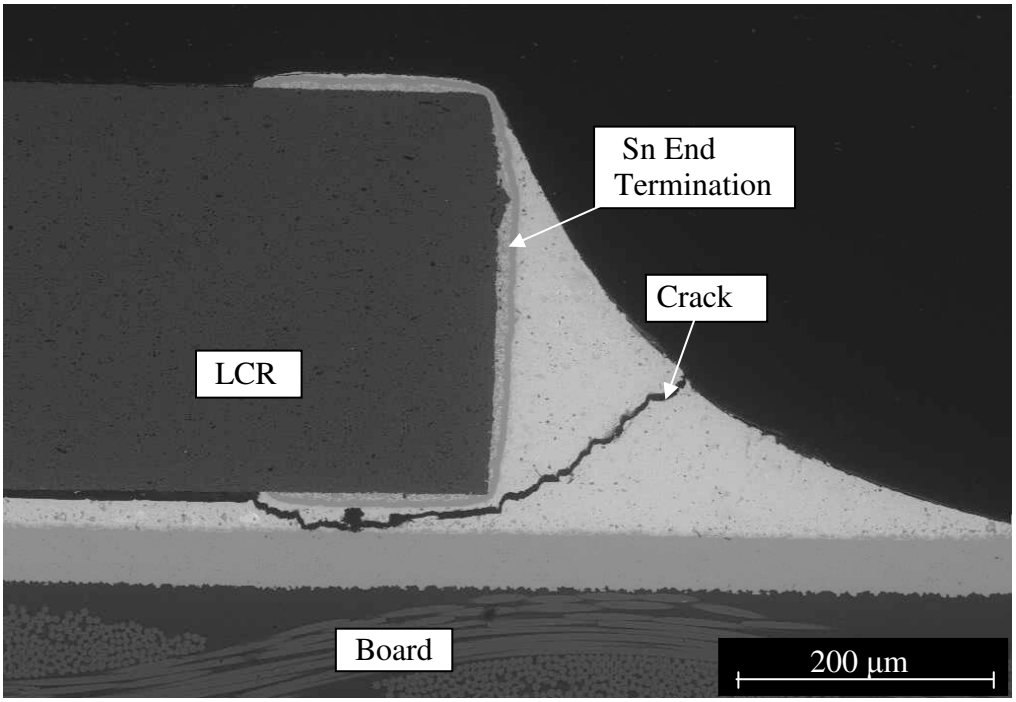

Figure 9 - SAC-ImSn after Aging at 125ºC for 100 hrs

Prior to conducting the destructive failure analysis, optical inspection of the 2512 LCRs was performed to identify failure locations. One of the observations that is present in Figure 10 is that the crack initiation point at the solder fillet varied within each interconnect. The cracks reached high points in the fillet, close to the component, and low points in the fillet that appear to be close to the copper pad in the board.

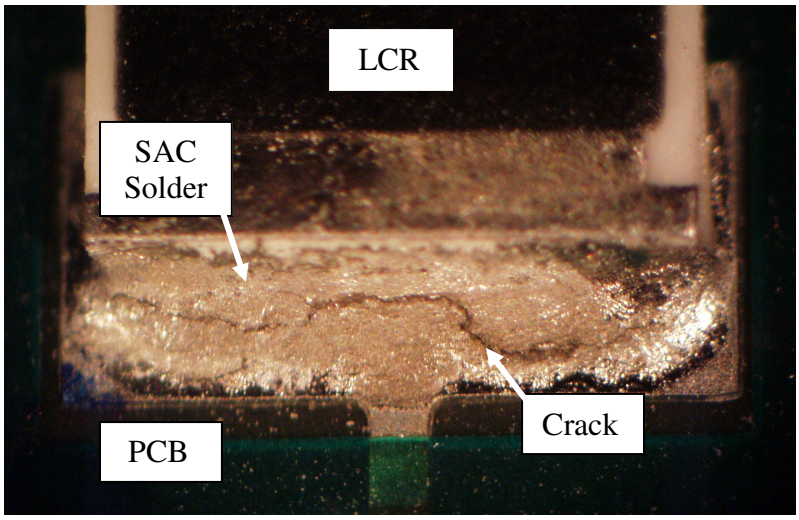

Figure 10 – Optical Image of SAC-ImAg Failure

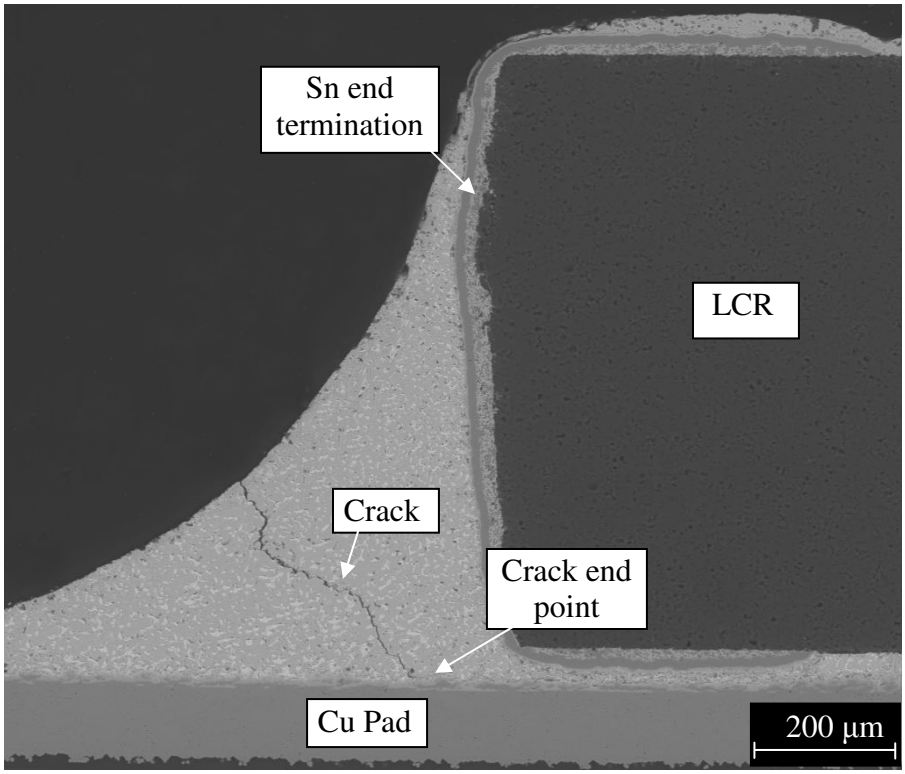

Figure 11 - Mixed-HASL after Aging at 125ºC for 100 hrs

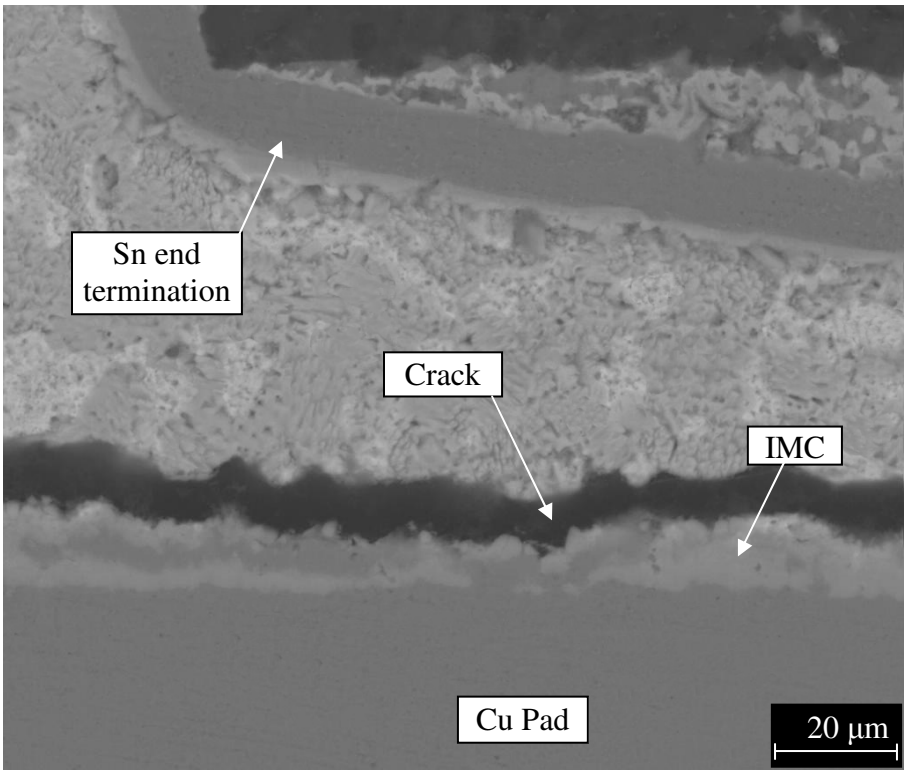

Figure 12 - Mixed-HASL after Aging at 125ºC for 100 hrs

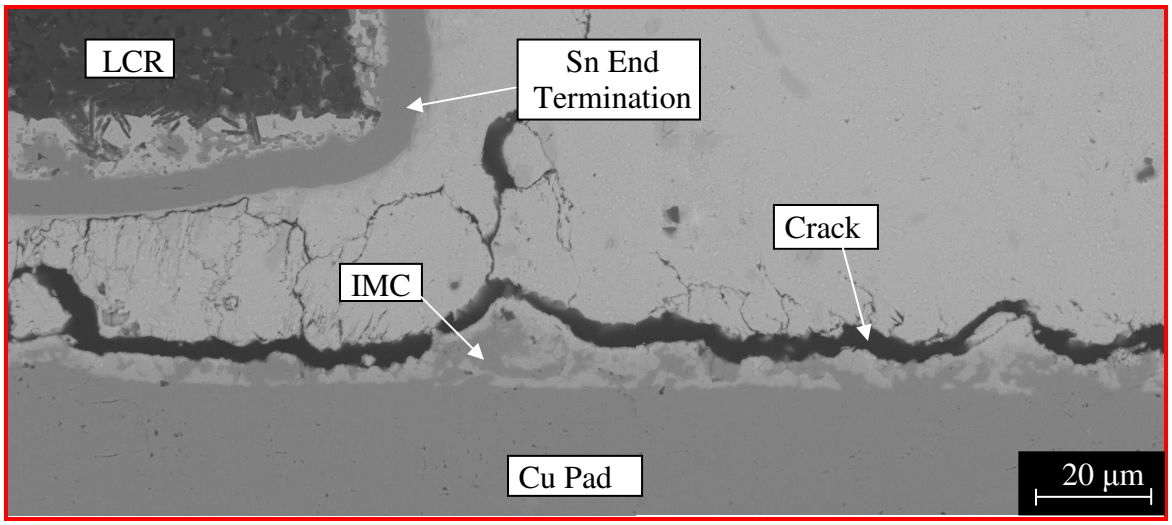

Figure 13 - SAC-ImAg after Aging at 125ºC for 100 hrs

The number of failed components and survived components from the assemblies that were examined is shown in Table BB. SnPb-HASL, Mixed-HASL, Mixed-ImSn and SAC-ImSn assemblies were found to have the largest number of failed components after performing failure analysis.

Table 5 – Failed and Survived Number of Samples

		Failed	Survived
SnPb-HASL		31/32	1/32
Mixed	HASL	13/16	3/16
	ImSn	16/16	0/16
	ENIG	10/16	6/16
SAC	ImSn	16/16	0/16
	ImAg	23/24	9/24
	ENIG	28/32	4/32
	OSP	11/16	5/16

Failure analysis also showed trace failures that may have caused electrical discontinuity. Figure 14 and Figure 15 are examples of sectioned solder joint where failure happened due to solder joint fatigue and trace cracking. In these images it is noticeable that the crack propagated through the solder, the copper trace and continued into the PCB. Figure 16 and Figure 17 show top views of the copper land and copper trace exposed after de-soldering and polishing the assembly. In both images, it is clear that cracks propagated across the copper trace outside the solder mask line. Although it is not possible to identify the cause of the initial electrical discontinuity that yielded to a TTF, all analysis and durability comparison will assume solder joint fatigue.

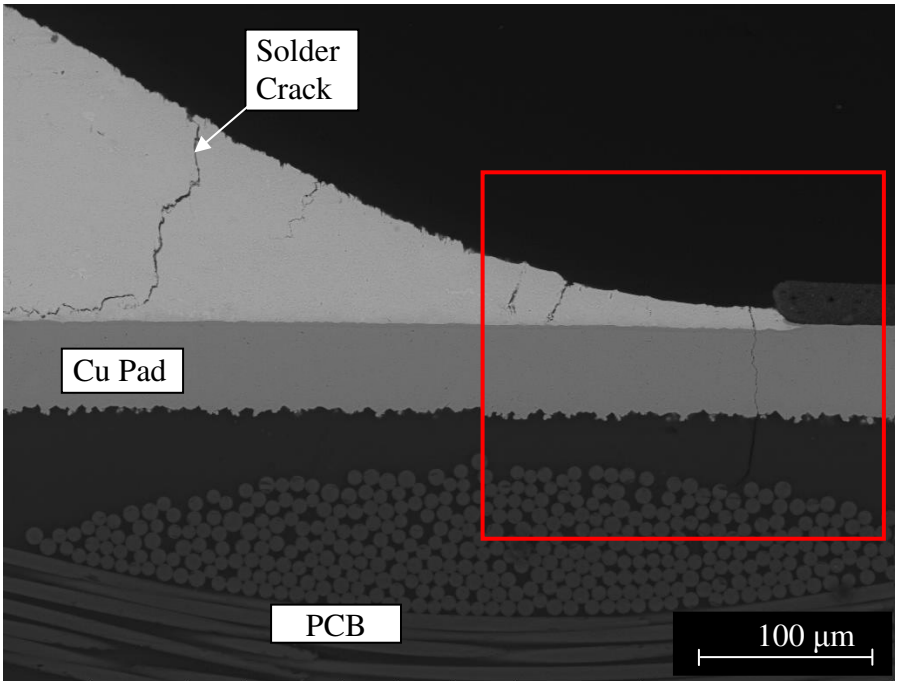

Figure 14 - Solder joint and Trace cracks

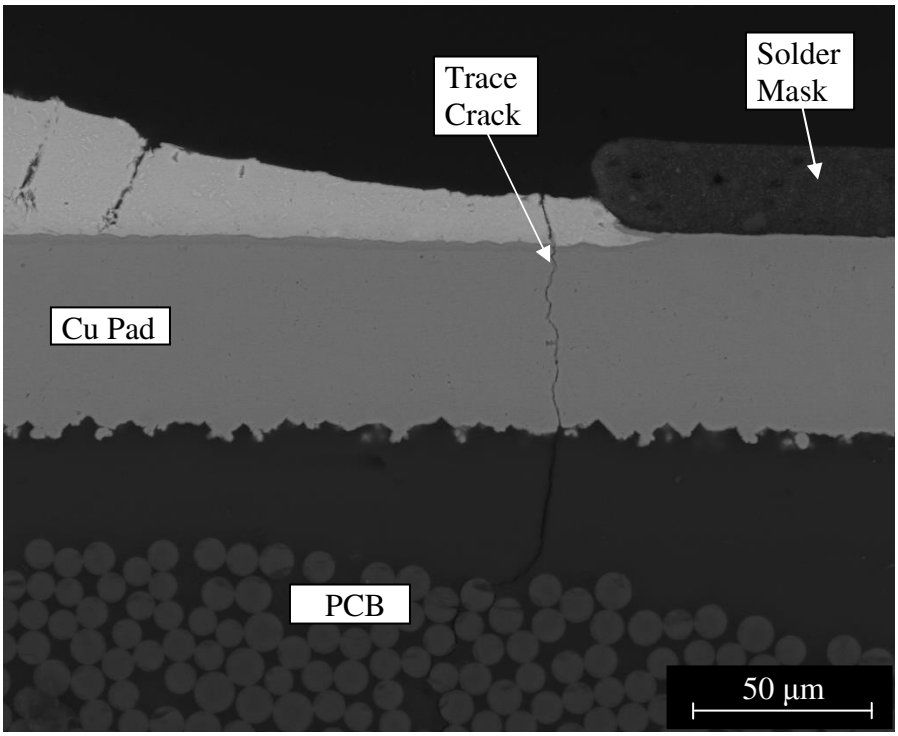

Figure 15 - Trace Crack

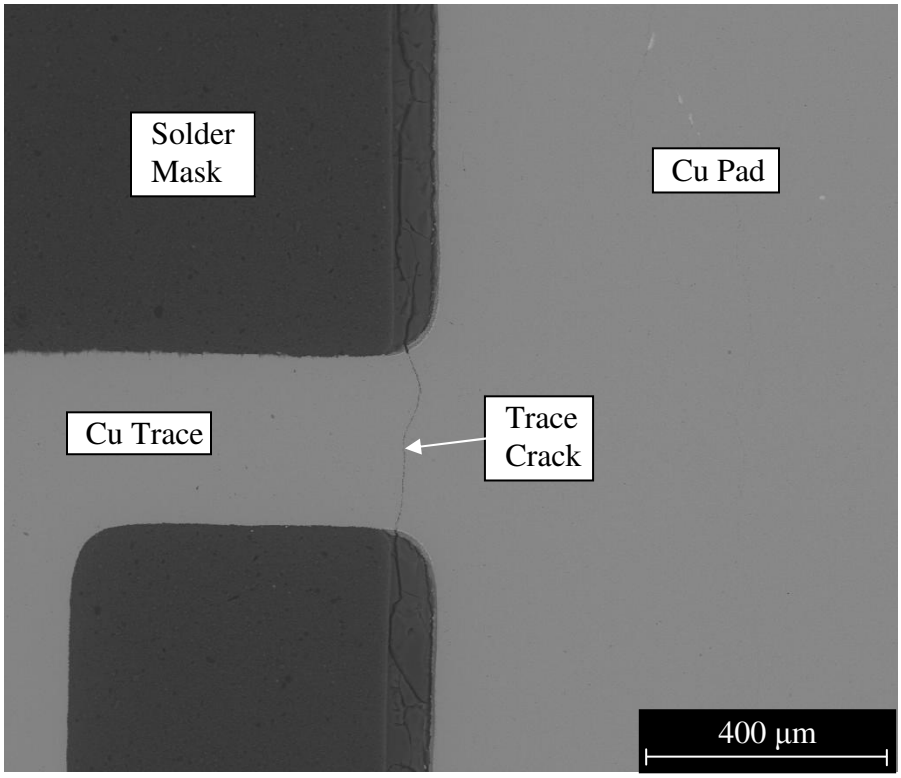

Figure 16 - Top view of trace crack

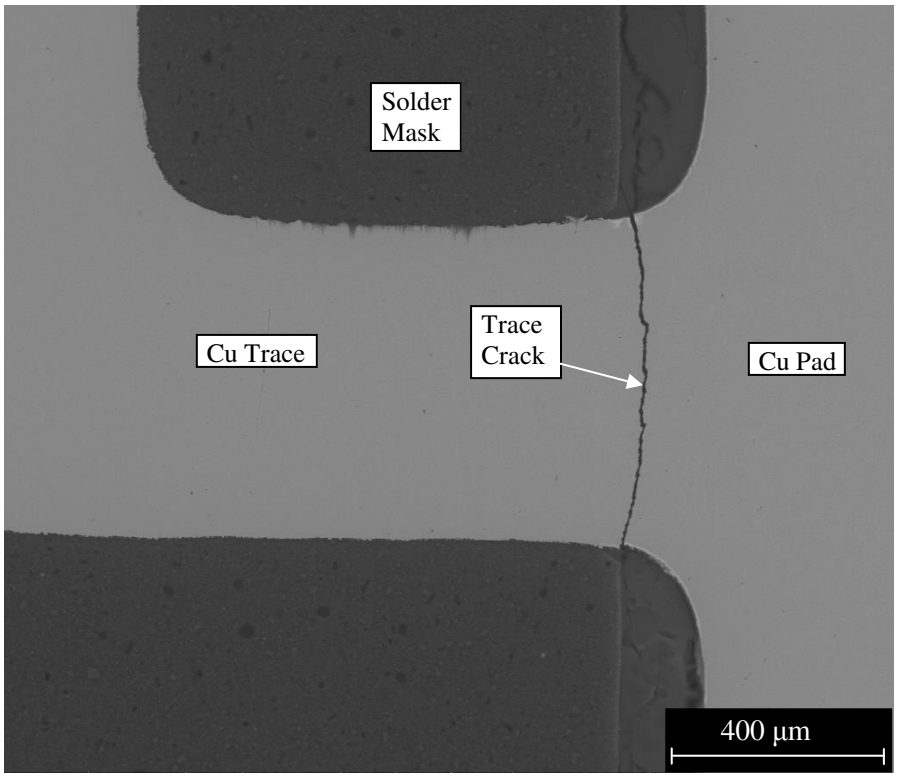

Figure 17 - Top view of trace crack

3.2 Test Results

The time to failure (TTF) data, in minutes, acquired from the random vibration test was analyzed using an analysis of variance (ANOVA). Rather than a comparison of the variances, this statistical tool compares the means of two or more groups by analyzing comparisons of variance estimates. In ANOVA, the null hypothesis is that the means of the groups are equal. If the null hypothesis is true, the populations compared are from the same population. This is estimated by comparing an F calculated versus and F critical. F critical is tabulated for a significant level of 5% while F statistics is equal to the ratio of the variance between groups (or mean square due to treatments) over the variance within groups (or mean square error). If the calculated value of F is equal to or larger than the critical F-value, then the null hypothesis is rejected which means that a significant difference exists in the populations compared.

The first step in the analysis of the TTF data is comparing the durability results for the mixed assemblies. Here, the F statistics of 5.59 is larger than the F critical of 2.65 implying that a significant difference exists among the populations. The ANOVA results are presented in Table 6.

Table 6 – Mixed Assembly ANOVA

Groups	*Count*	*Sum*	*Average*	*Variance*
Mixed-HASL	8	47511	5938	15182470
Mixed-ImSn	7	43549	6221	41226437
Mixed-ImAg	8	177982	22247	441232655
Mixed-ENIG	8	2009505	251188	7.52E+10
Mixed-OSP	8	44765	5595	15730936

ANOVA

Source of Variation	*SS*	*df*	*MS*	*F*	*P-value*	*F crit*
Between Groups	3.71E+11	4	9.28E+10	5.95	0.001	2.65
Within Groups	5.30E+11	34	1.56E+10			
Total	9.01E+11	38				

The comparison of the TTF data of the mixed assemblies with different finishes against SnPb-HASL revealed that Mixed-ImAg and Mixed-ENIG were significantly different from the SnPb-HASL results whereas Mixed-HASL, Mixed-ImSn and Mixed-OSP showed no statistical difference with SnPb-HASL TTF data. Further, ANOVA showed no significant statistical difference between Mixed-ImAg and Mixed-ENIG with an F critical of 4.6 bigger than F calculated of 1.37.

The ANOVA was also applied to the TTF obtained from the lead-free assemblies. The results presented in Table 7 show that no significant difference is found among the lead-free assemblies. These results indicate that the specific lead-free board pad finishes were

not found to significantly influence the vibration durability of the SAC soldered assemblies.

Table 7 – SAC ANOVA

Groups	Count	Sum	Average	Variance
SAC-ImSn	8	7413	927	1838
SAC-ImAg	6	4120	687	109137
SAC-ENIG	7	5472	782	10248
SAC-OSP	8	7490	936	36610

ANOVA

Source of Variation	SS	df	MS	F	P-value	F crit
Between Groups	298370	3	99457	2.837	0.058	2.99
Within Groups	876312	25	35052			
Total	1174682	28				

After comparing the SnPb-HASL results versus each individual lead-free assembly using ANOVA, it was found that the reliability of these solder joint materials does not have a significant difference when tested under random vibration conditions. Results are summarized in Table 8.

Table 8 – ANOVA comparison between SnPb-HASL and lead-free assemblies

	F statistics	**F critical**	**Result**
SAC-ImSn	0.58	4.75	No significant difference
SAC-ImAg	4.41	4.6	No significant difference
SAC-ENIG	0.01	4.67	No significant difference
SAC-OSP	2.48	4.6	No significant difference

3.3 Data Adjustment

While the same vibration step stress loads were applied to all assemblies, the question of comparing test data over multiple load conditions which impose different damage rates may be raised. To address this concern, the TTF data may be adjusted. To accomplish the adjustment, the empirical model derived by Steinberg [10] to estimate the interconnect fatigue life under vibration environments is used.

The time that a component interconnect would survive under a random vibration environment, if the magnitude of the stress is held at constant excitation level, i.e., N, can be calculated using Basquin's Power Law. This model is accepted in the research community as a simple relationship that addresses failures under high cycle fatigue. The stress-life model states,

$$\sigma * N^{b} = C \qquad \textbf{Equation 3.1}$$

where σ is the stress amplitude, N is the number of stress cycles to failure, C and b are material constants. Under the assumption that solder joint stress is directly proportional to the displacement of the board (Z) where the component is attached [10], equation 1 can be re-written as

$$Z * N^{b} = Const. \qquad \textbf{Equation 3.2}$$

In developing a model, Steinberg also identified a position factor. This position factor is a normalized value that relates to the curvature at the component position, which can be referred to as the relative curvature (Ri). The Ri value is the curvature at a specific position divided by the maximum observed curvature on the board. Initially, the value Z1

is assumed to correspond to the position of highest board curvature. Thus, Ri is used as an adjustment factor to account for the displacement experienced at different positions. As a result, Basquin's relationship can be expressed as

$$N_2 = N_1 * \left(\frac{Z_1}{Z_2 * R_i} \right)^{\frac{1}{b}}$$ **Equation 3.3**

Z1 and Z2 have been empirically modeled by Steinberg in his studies,

$$Z_1 = \frac{0.00022 * B}{C * h * \sqrt{L}}$$ **Equation 3.4**

and

$$Z_2 = \frac{36.85 * \sqrt{PSD}}{f_n^{1.25}}$$ **Equation 3.5**

Where B is the length of the PWB unsupported edge, L is the length of the electronic component, h is the board thickness, PSD is the power spectrum density level at the natural frequency of the assembly measured in G^2/Hz, f_n is the natural frequency of the board, and C is the component type constant. Substituting Equation 3.4 and Equation 3.5 into Equation 3.3 results in an estimation of the time to failure of a component under random vibration:

$$N_f = N \left[\frac{f_n^{1.25} * 0.00022 * B}{R_i * 36.85 * C * h * \sqrt{L * PSD}} \right]^{\frac{1}{b}}$$ **Equation 3.6**

The first step in the adjustment of the TTF data collected during the vibration step-stress test is to adjust to a common load level. Since the natural frequency and relative

curvature of a board does not change as the magnitude of the vibration load is changed, the acceleration factor between load level i and j using equation 6 can be expressed as

$$A_{f\,i-j} = \frac{N_i}{N_j} = \left[\frac{\sqrt{PSD_j}}{\sqrt{PSD_i}}\right]^b \qquad \textbf{Equation 3.7}$$

Strain history in the time domain collected during the vibration test was transferred to the frequency domain using Fast Fourier Transform to estimate the dynamic response of each of the tested boards. Since the frequency of the boards varied slightly due to position and clamping force in the fixture, the TTF data was adjusted to the lowest Natural Frequency recorded, 180 Hz, for each position of the components of interest in this work. To accomplish this task, the TTF data is multiplied as following:

$$N_{normalized} = N_i * \left[\frac{R_{xy} * f_{ni}^{1.25}}{180^{1.25} * R_i}\right]^b \qquad \textbf{Equation 3.8}$$

3.4 FEA Global Model

To calculate the relative curvature of the board at the individual component positions, Finite Element Analysis (FEA) was performed using calcePWA® which is a software used to estimate circuit assemblies failures [28]. Figure 18 and Figure 19 show an example of the strain history over a span of 250 micro-seconds and response of a test vehicle in the frequency domain, respectively.

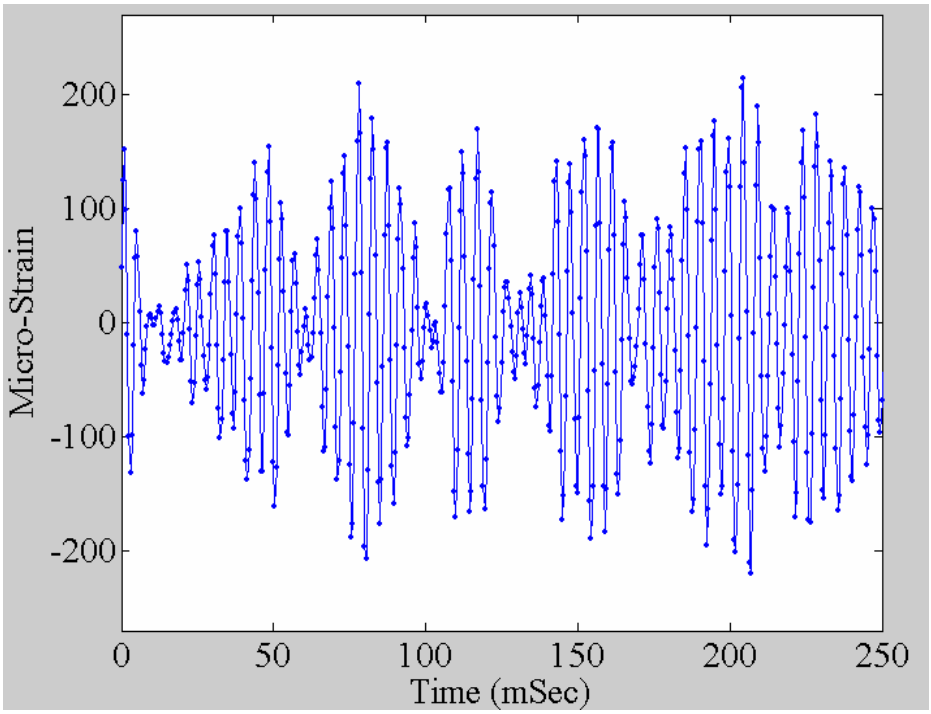

Figure 18 - Strain Measurement in Time Domain

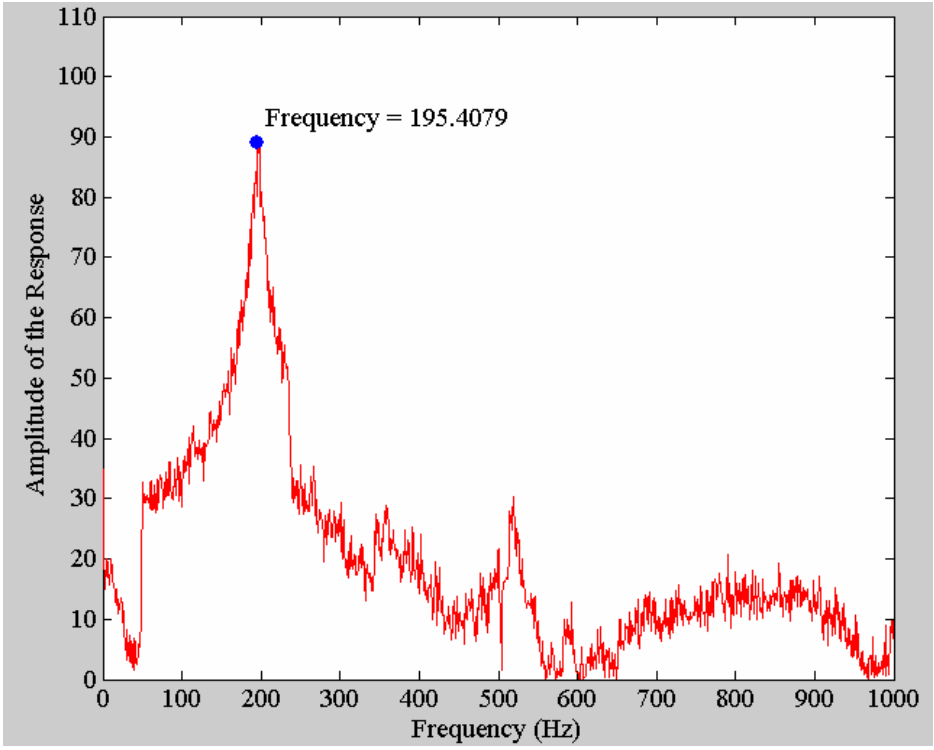

Figure 19 –Amplitude Spectrum of Strain Response

The frequency response of all the test vehicles that were tested in this study is presented in Table 9. Since the variation in the response of the PWBs is due to clamping of the test vehicles and their location in the fixture, the Y-axis Rotational Spring Constant in the FEA was adjusted so that the finite element model matched the measured frequency response of the PWBs.

Table 9 – Frequency Response of the Tested Boards

Assembly		f_n **(Hz)**
SnPb-HASL	Board 1	184
	Board 2	196
SAC-ImSn	Board 3	180
	Board 4	197
SAC-ImAg	Board 5	197
	Board 6	197
SAC-ENIG	Board 7	210
	Board 8	204
SAC-OSP	Board 9	195
	Board 10	189
Mixed-HASL	Board 11	195
	Board 12	189
Mixed-ImSn	Board 13	194
	Board 14	193
Mixed-ImAg	Board 15	193
	Board 16	202
Mixed-ENIG	Board 17	229
	Board 18	221
Mixed-OSP	Board 19	201
	Board 20	200

Figure 20 shows the model of the test vehicle in calcePWA®. After performing the vibration analysis and matching each frequency response, the board curvature values were calculated. Figure 21 shows the board curvature that will be used in the adjustment of the data.

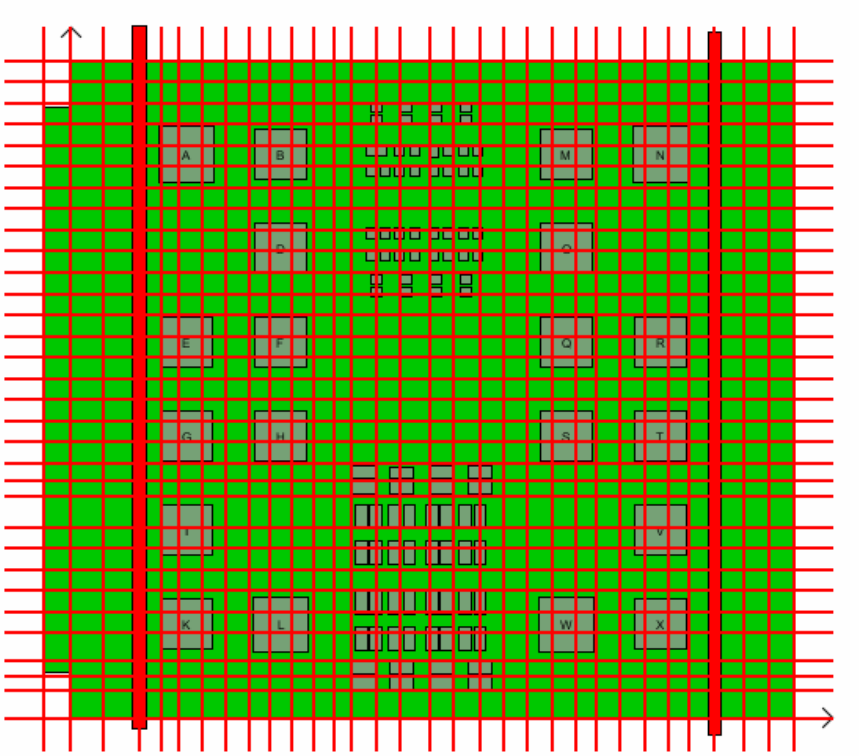

Figure 20 – calcePWA® Global Model

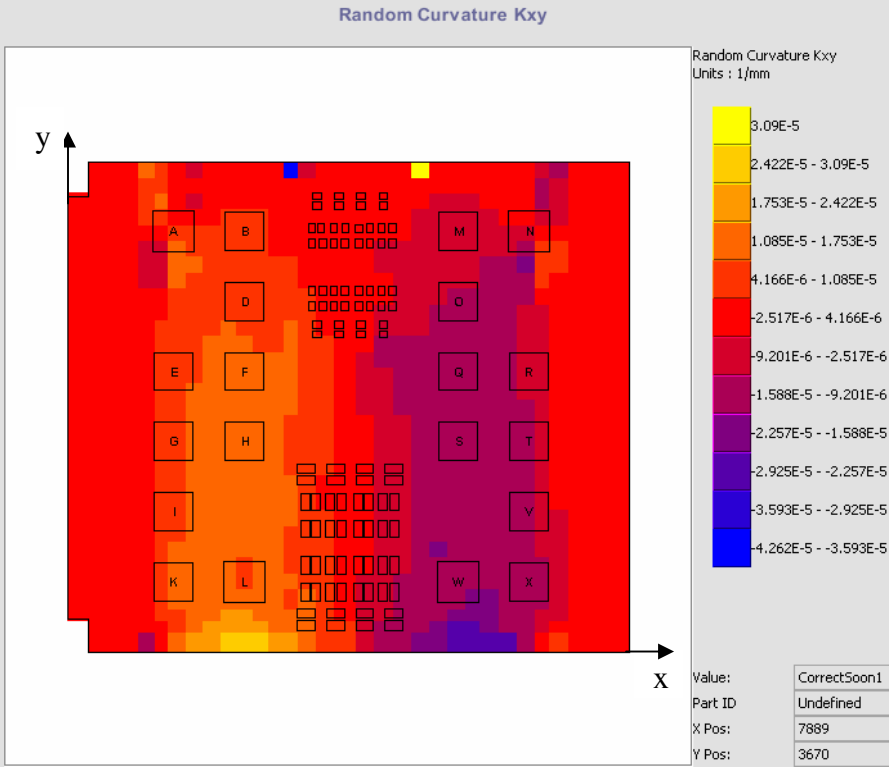

Figure 21 – calcePWA® Board Curvature

The non-destructive failure analysis identified failures on interconnects of LCR components that positioned parallel to the non-clamped edges of the PWB (see Figure 1). The sixteen components are distributed among four daisy chains. In the non-destructive failure analysis it was found that the components that failed more frequently are those outlined in red; therefore, the TTF that was recorded for the four daisy chains in all 10 boards tested will be assigned to components 1, 3, 9 and 11 in Figure 22. The objective of assigning the TTF to a specific component is to be able to calculate the relative curvature to a specific relative curvature that will be calculated in calcePWA®. In addition, the vibration analysis yielded a solution that confirms this assumption. The components that failed first, among these 16 components that are distributed in the 4

daisy chains, match these same 4 positions. The relative curvatures for positions 1, 3, 9 and 11 as function of board frequency are plotted in Figure 23.

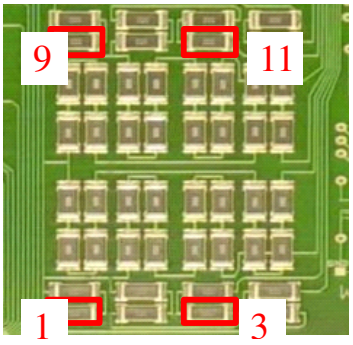

Figure 22 – 2512 LCR Component Distribution

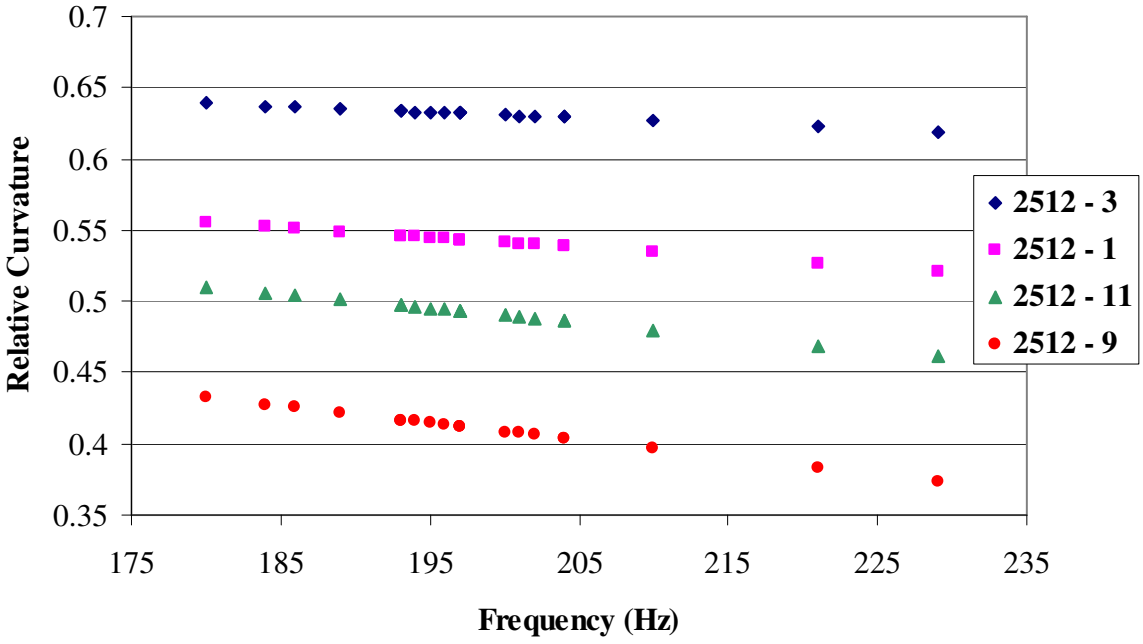

Figure 23 – Board Relative Curvature as a Function of Natural Frequency

3.5 Analysis of Variance

Once TTF data was adjusted to a common load level for all failed 2512 LCRs, analysis of variance (ANOVA) was performed once again. As indicated with the non-adjusted TTF data, a significant difference in TTF data was indicted among the mixed and SnPb assemblies. Here, the F statistics is 5.95 while the F critical is 2.65. Therefore, the adjusted TTF data from each mixed assembly is compared to the SnPb-HASL data to verify which assembly differs from SnPb-HASL results. ANOVA comparison of SnPb-HASL versus Mixed-HASL resulted in an F-critical of 4.6 and F-calculated of 2.45. These results indicate that the influence of the different end terminations (Sn for mixed-HASL and SnPb for SnPb-HASL) on the 2512 resistors cannot be observed in the variance of the adjusted TTF data. The ANOVA comparisons between SnPb-HASL and the mixed assemblies are presented in Table 10. Since the bulk solder of these interconnects is the same and the end termination does not influence the durability of the interconnect, board pad finishes of ImSn and OSP cannot be distinguish when compared to HASL.

Table 10 – ANOVA between SnPb and SAC assemblies

	F statistics	**F critical**	**Result**
Mixed-HASL	2.45	4.60	No significant difference
Mixed-ImSn	1.55	4.67	No significant difference
Mixed-ImAg	6.6	4.60	Significant difference
Mixed-ENIG	6.56	4.60	Significant difference
Mixed-OSP	1.91	4.60	No significant difference

The influence of the board termination under vibration environments was also studied using the adjusted TTF data from the lead-free assemblies. The ANOVA results yielded an F statistics of 1.14 and an F critical of 2.99 implying no significant difference among TTF data for the various lead-free board pad finishes assembled with SAC solder. Comparing these results with the mixed results, it can be concluded that ImAg and ENIG have an effect on the vibration reliability of the LCR interconnect when SnPb solder is used while there is no influence when SAC solder is used. Further, there appears to be no significant difference between the TTF data for SAC-ImSn, SAC-OSP, SAC-ENIG, SAC-ImAg, SnPb-HASL, Mixed-HASL, Mixed-ImSn and Mixed-OSP.

ANOVA was then applied to determine whether there is difference in the durability of grouped SnPb vs. the grouped lead-free assemblies. The lead-free data was compared, individually, with the SnPb-HASL data. The results obtained, summarized in Table 11, indicate that, excluding SnPb-ImAg and SnPb-ENIG, no significant difference exits between the durability of Sn3.0Ag0.5Cu and Sn37Pb solder joints when tested under defined vibration conditions.

Table 11 – ANOVA between SnPb and SAC assemblies

	F statistics	**F critical**	**Result**
SAC-ImSn	0.002	4.75	No significant difference
SAC-ImAg	2.01	4.6	No significant difference
SAC-ENIG	0.19	4.67	No significant difference
SAC-OSP	1.94	4.6	No significant difference

Although ANOVA estimates whether there is a significant difference between two or more populations, the analysis does not point out where there difference between the populations falls. To achieve so, weibull plots were generated using the adjusted TTF to compare the 10 percent failure (in this case, the first failure) between the mixed soldered assemblies versus SnPb-HASL and the SAC soldered assemblies versus SnPb-HASL.

Figure 24 and Figure 25, show the least reliable assemblies are SnPb-HASL and the ImSn assemblies followed by the OSP board pad finish assemblies. On the other hand, the mixed and SAC assemblies that appeared to have the best durability results are those assembled with ENIG and ImAg.

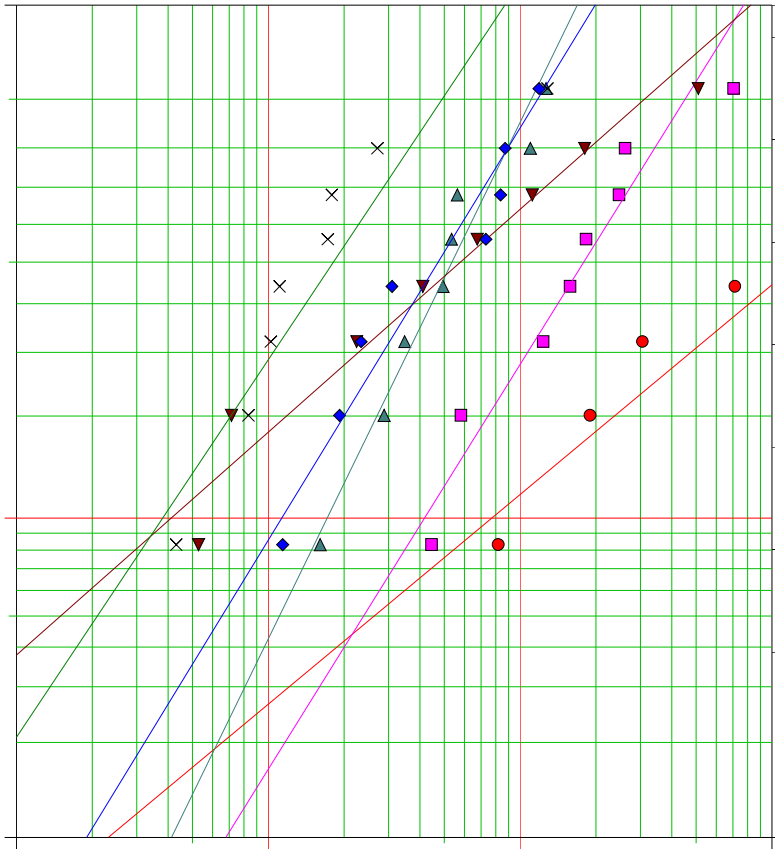

Figure 24 – Weibull Mixed vs. SnPb-HASL

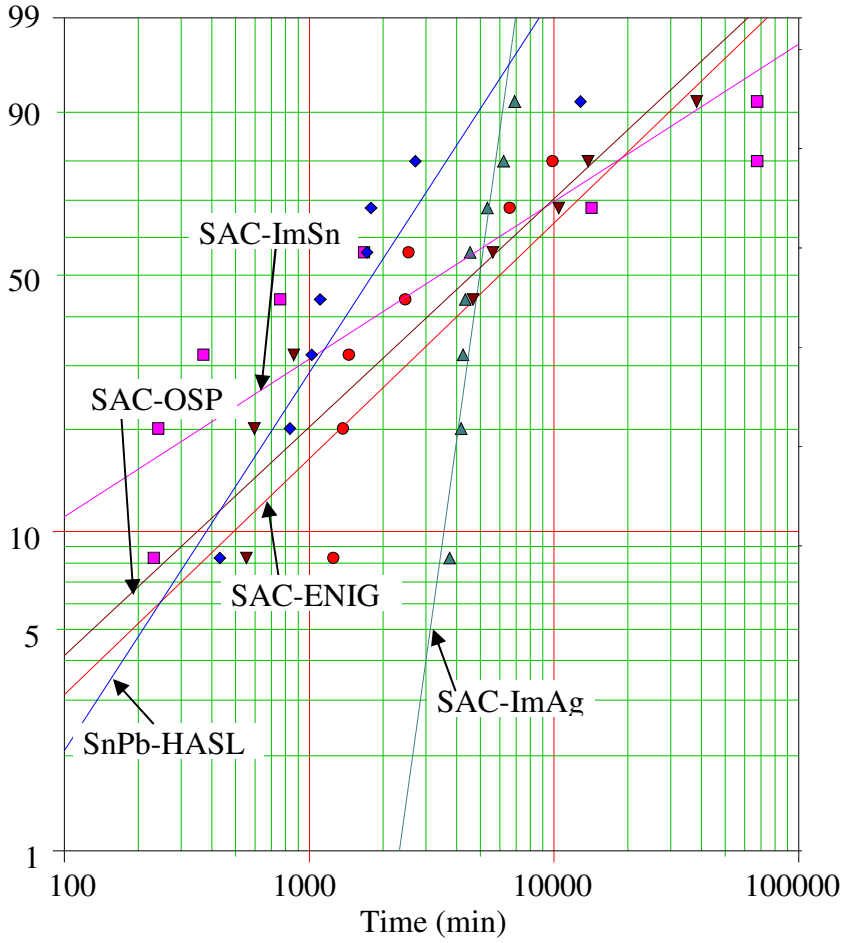

Figure 25 – Weibull SAC vs. SnPb-HASL

Chapter 4: Conclusions, Contributions and Future Work

In this chapter, a summary of the work will be presented. Section 4.1 presents a summary of the test procedure, failure analysis findings and conclusions of the work. The contributions of this work to the industry and academia are presented in section 4.2. Suggestions for future work are presented in section 4.3.

4.1. Conclusions

Electronic assemblies are often subjected to random vibration environments depending on their application. Therefore, random vibration tests are being used to qualify and evaluate electronic assemblies. This thesis provides a durability assessment of SnPb and SnAgCu solder interconnects of surface mount resistor tested using an out-of-plane random vibration. The random vibration was applied through an increasing four step-stress profile. Tests variables for a common test design included solder material, component terminal finish, and board pad finish.

The 2512 leadless chip resistors identified as failed during the random vibration test due to an increase in the measured electrical resistance were subjected to destructive failure analysis. Two failure mechanisms were identified. First, solder joint fatigue failures were observed for SnPb, mixed and SAC assemblies. The failures observed revealed a difference on the propagation path of the cracks between the SnPb and the lead-free (SAC) and mixed (SnPb) solder assemblies. In all cases, the cracks propagated into the fillet and through the bulk solder above the interfacial intermetallics. When the crack reached the 2512 component, the crack path in the SnPb-HASL moved from the bulk

solder into the metal termination of the LCR and then along the interface between the ceramic part body and the metal terminal. For the Sn-finish terminal parts, the crack remained on the bulk solder. The unique crack path on the SnPb-termination LCRs may be due to the larger terminal size of the SnPb finished 2512 terminals as compared to the 2512 components with the Sn-finish terminals. The second failure mechanism identified was cracks that propagated through the copper traces, the copper trace and continued into the PCB. The cracks observed, were located across the copper trace beyond the solder mask line. Even though it is not possible to identify which failure mechanism caused the TTF of the daisy chains tested, the statistical analysis performed to compare the durability of SnPb, mixed and SAC assemblies assumed solder joint fatigue.

A random vibration fatigue model was used to adjust all time to failure (TTF) data to a common load level. Weibull plots and the ANOVA performed in this study yielded interesting conclusions regarding the random vibration durability of the leadless chip resistors as a function of solder material, board pad finish and component end termination. First, the ANOVA showed that no significant difference in the TTF data was found due SnPb and Sn finished terminations for tin-lead soldered assemblies. The TTF data for SnPb solder assemblies with ImAg and ENIG board pad finishes were found to be significantly different than the assemblies with other board pad finish and solder treatments. These two finishes were found to be more reliable on average that the other finishes when assembled with tin-lead solder. The tested lead-free board pad finishes were indistinguishable in TTF of SnAgCu soldered assemblies as ANOVA results suggested. No significant durability difference was found between the Sn37Pb-

HASL results and the Sn3.0Ag0.5Cu results when tested under stepped random vibration environments. Weibull plots, on the other hand, were used to find where the differences between these populations lie. The 10th unreliability percentile showed that, under the tested random vibration conditions, the 2512-LCR assemblies solder with SnAgCu and SnPb on board pad finishes ImAg and ENIG were the most durable assemblies.

4.2.Contributions

Although the literature shows that random vibration loading has been used to study the reliability of solder joints, this work aslo focuses on the impact of different factors that influence the reliability of a solder joint interconnect.

- This study first systemically studied the durability comparison of tin-lead versus tin-silver-copper solder joint using the 2512 leadless chip resistor under random vibration loading conditions.
- The impact of the end termination metallization (SnPb and Sn) on the reliability of leadless chip resistors assembled with tin-lead solder paste are tested and compared under random vibration loading.
- The influence of the board pad finish on the durability of different solder systems is studied under random vibration loading. Tin-lead soldered components onto hot air solder leveling pad finish served as baseline in the comparison of the durability of tin-lead and tin-silver-copper soldered components onto lead-free board pad finishes.

4.3.Suggestions for Future Work

In this section, suggestions are provided for future random vibration durability tests that can be conducted to corroborate and support the findings presented in this thesis work.

- The failure analysis conducted in this study identified a failure location that is not related to solder joint fatigue. Therefore, a new test vehicle should be designed in order to ensure that net failures will be caused by solder fatigue.
- Due to the implementation of a step-stress profile to accelerate fatigue failures under random vibration, it would be interesting to verify whether these results remain true with a single load level test. This test would validate the TTF adjustment procedure that was conducted in the study.
- The failure analysis conducted in this study revealed a difference between crack propagation paths between SnPb assemblies and SAC assemblies. It is suggested that a local finite element analysis is performed to verify and explain this difference.
- This study only focused on the reliability evaluation of leadless chip resistors of size 2512 although the test vehicle used included grid ball arrays (BGA), quad-flat packages (QFP) and resistors of size 1210. Future work related to this study should include processing and analysis of the data collected from this packages.
- A metallurgical explanation of the improved vibration fatigue life for SnPb-ImAg and SnPb-ENIG should be performed.

Appendices

APPENDIX A – Additional Failure Analysis in Section 3.1

A.1 SnPb – HASL

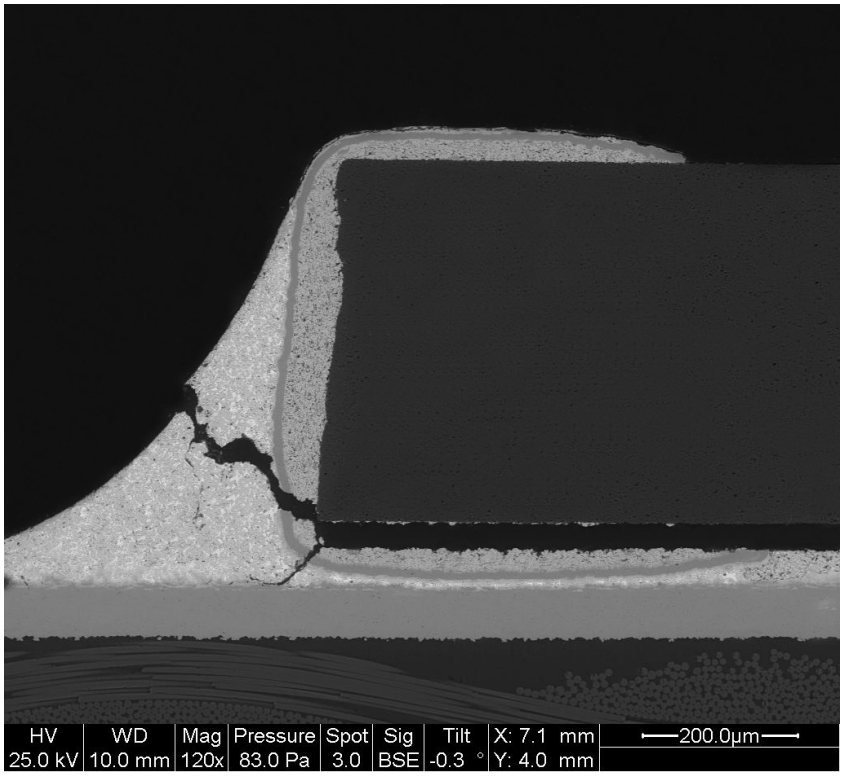

Figure A.1. 1 – SnPb-HASL

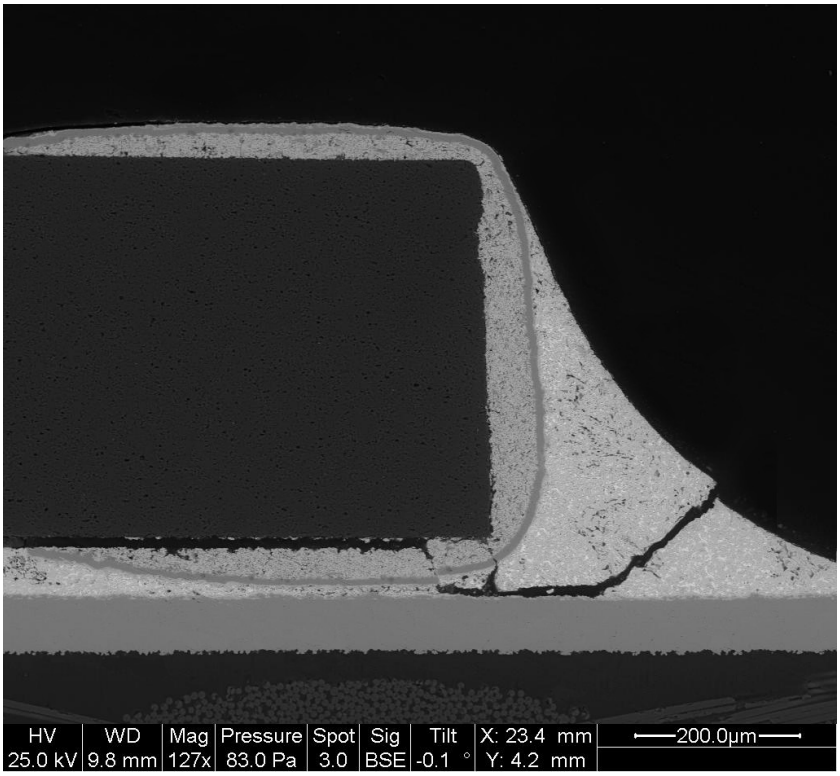

Figure A.1. 2 – SnPb-HASL

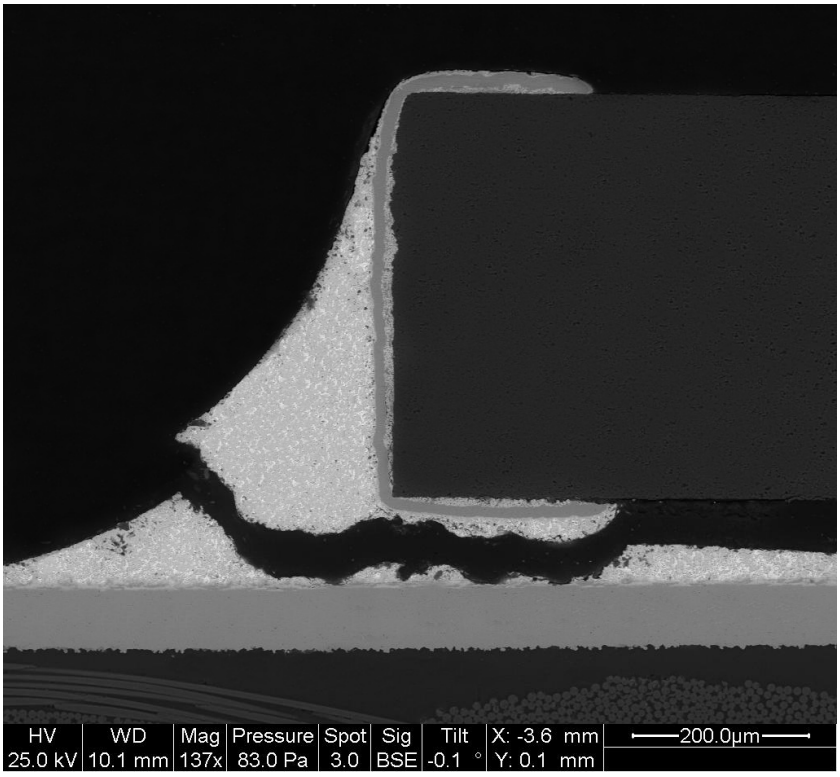

Figure A.1. 3 – SnPb-HASL

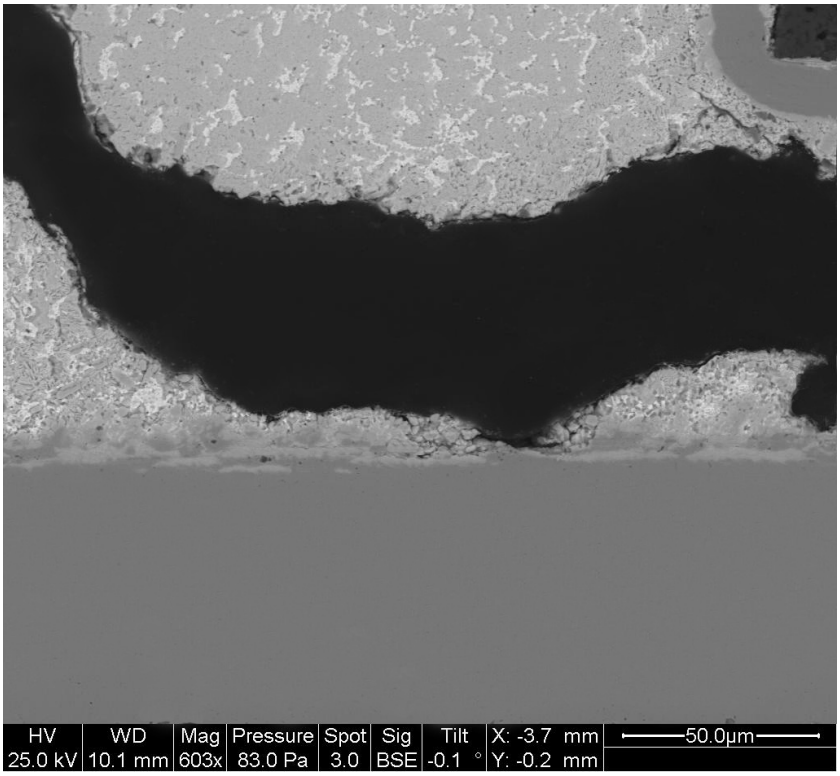

Figure A.1. 4 – SnPb-HASL

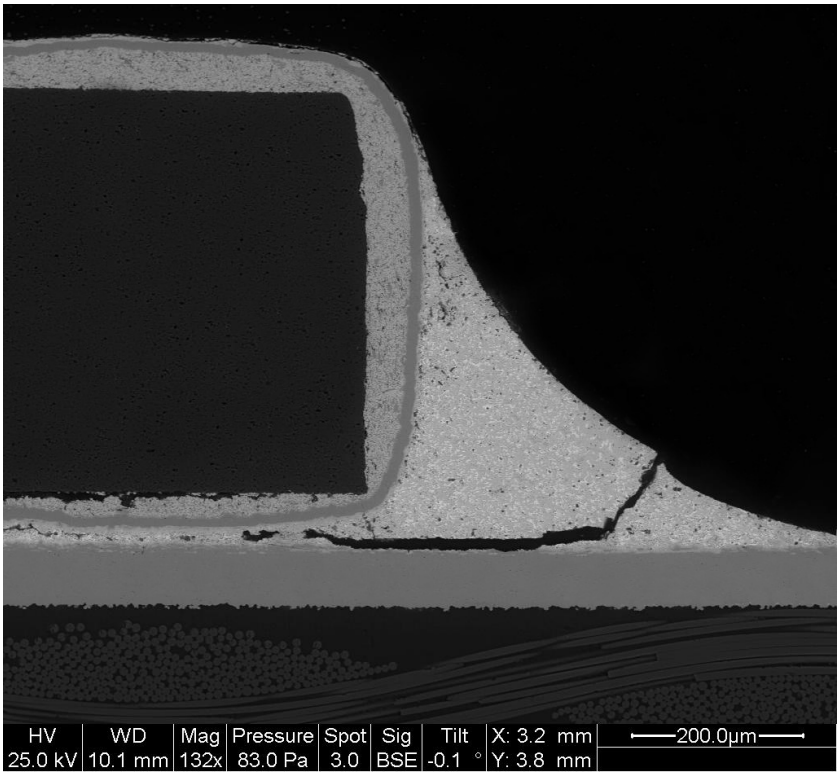

Figure A.1. 5 – SnPb-HASL

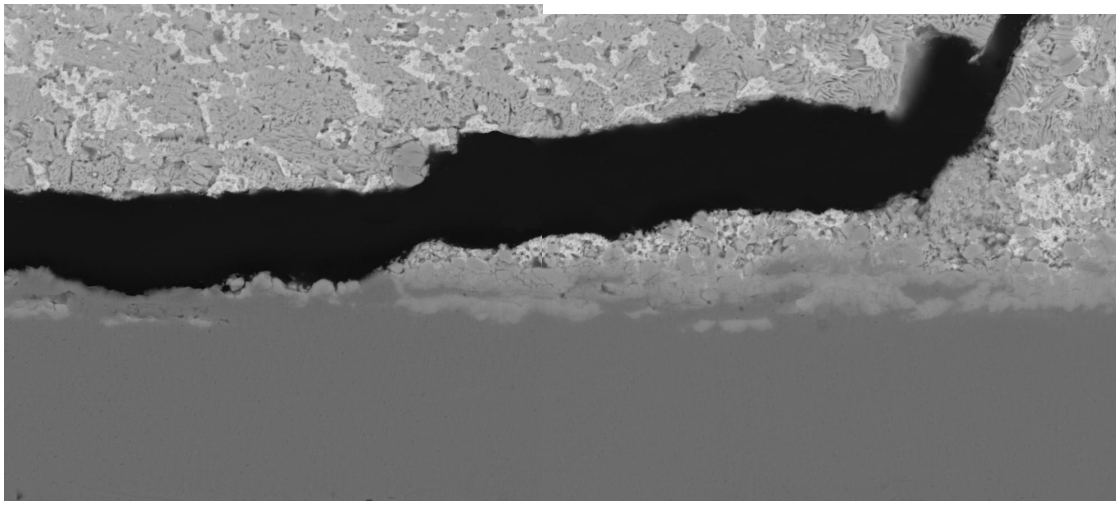

Figure A.1. 6 – SnPb-HASL

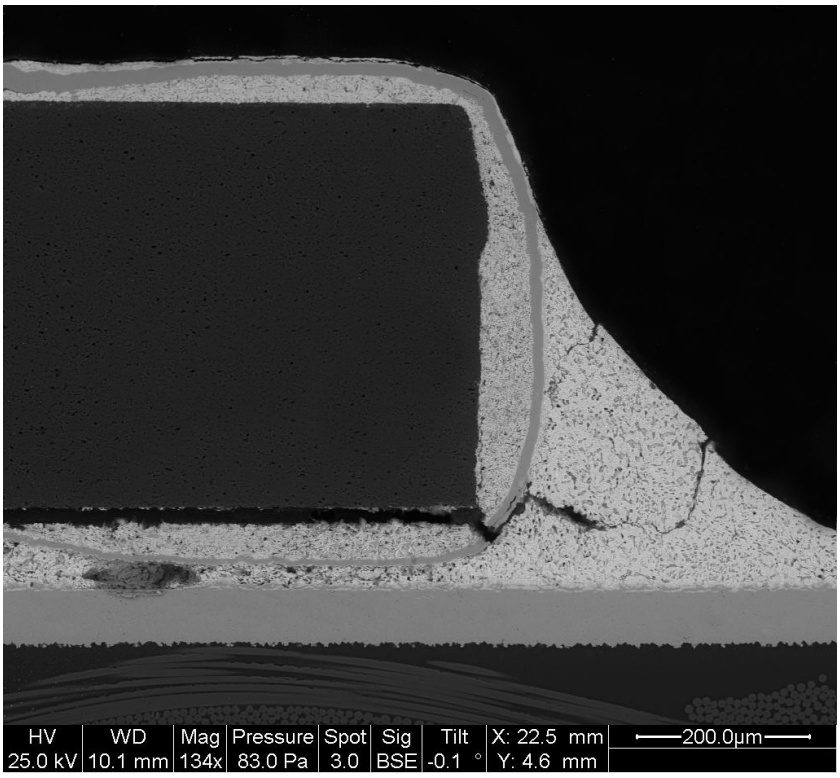

Figure A.1. 7 – SnPb-HASL

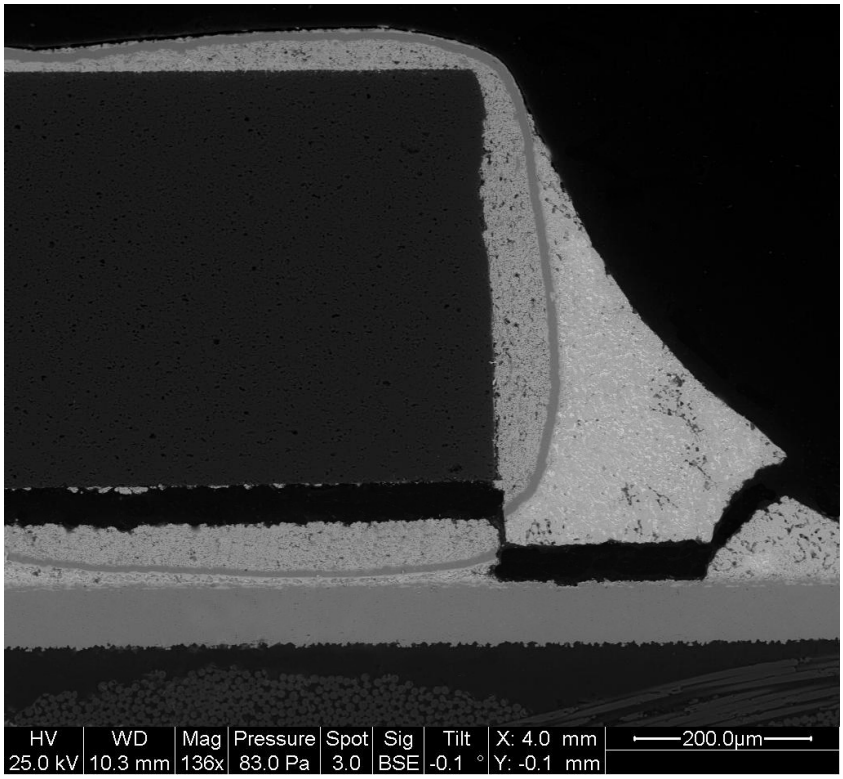

Figure A.1. 8 – SnPb-HASL

A.2 Mixed – HASL

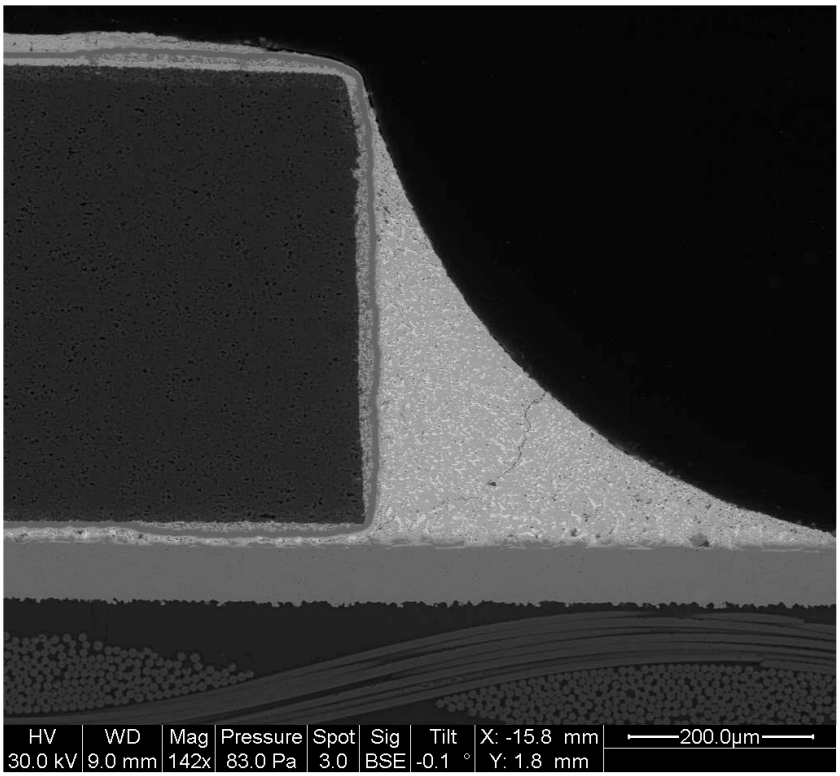

Figure A.2. 1 – Mixed-HASL

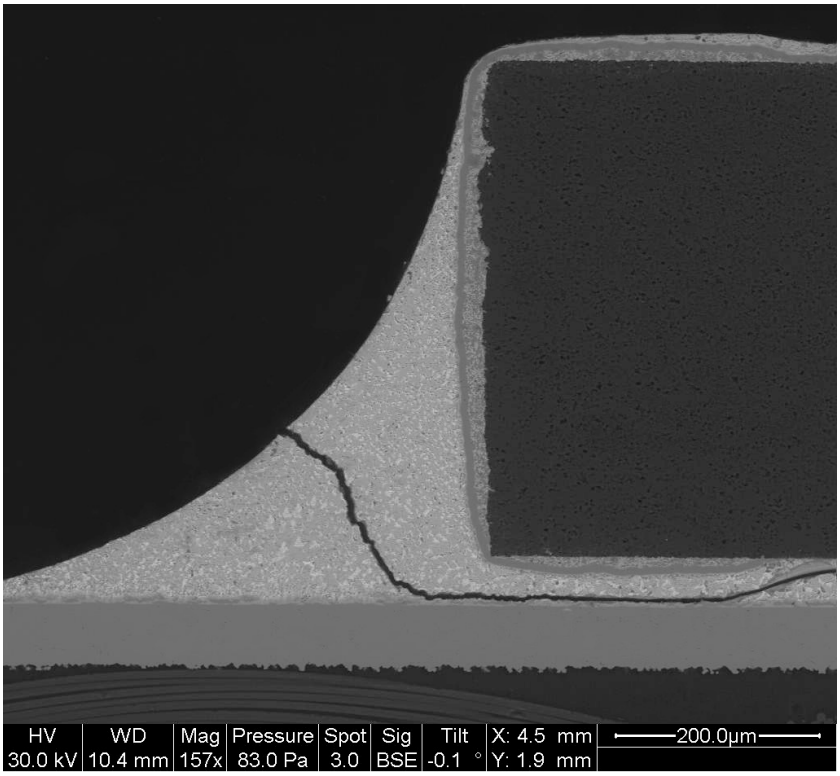

Figure A.2. 2 – Mixed-HASL

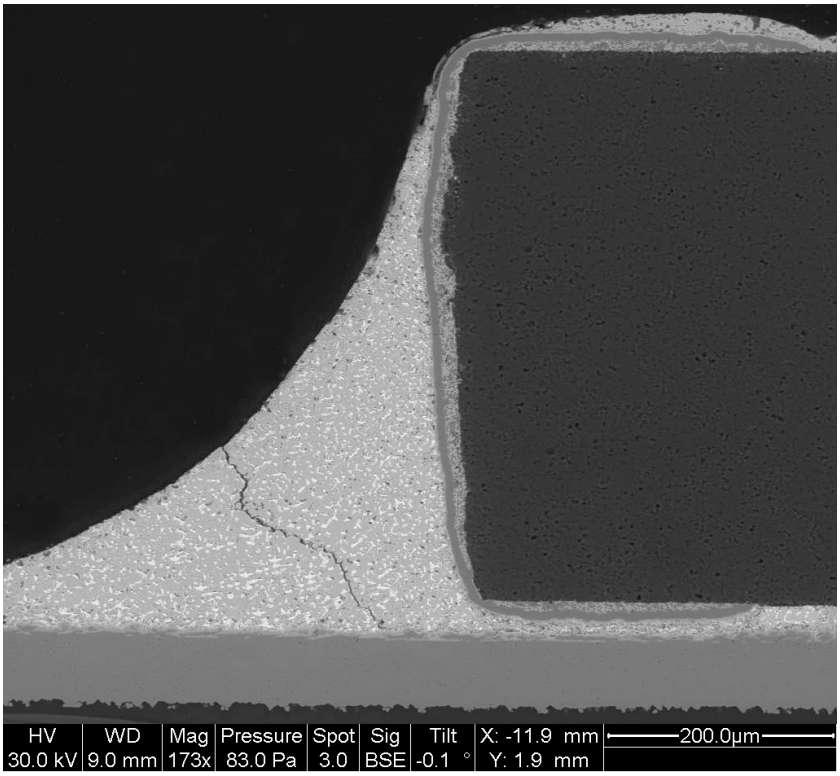

Figure A.2. 3 – Mixed-HASL

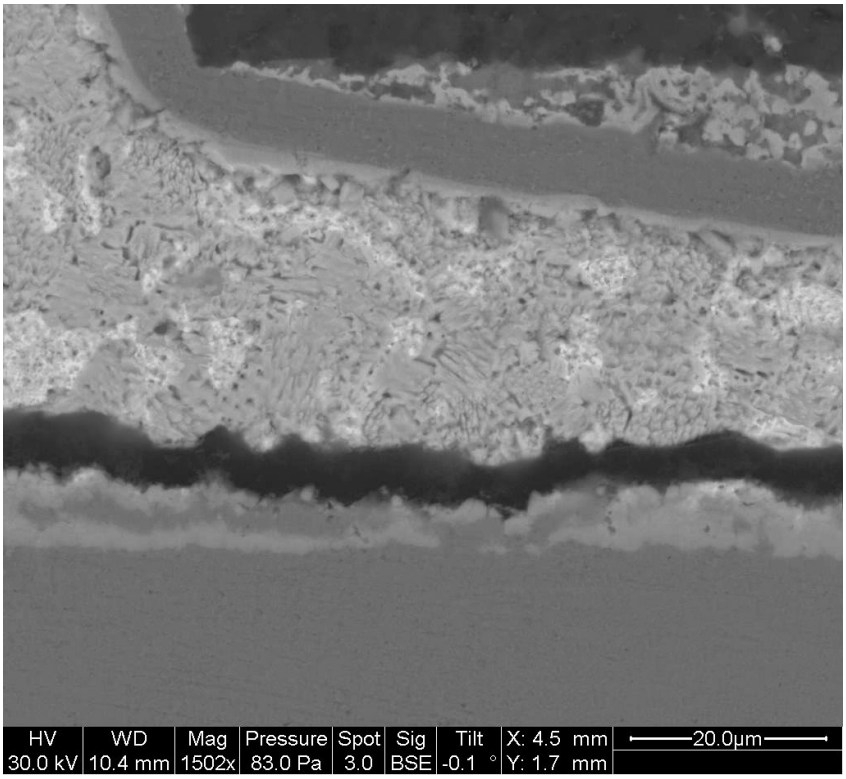

Figure A.2. 4 – Mixed-HASL

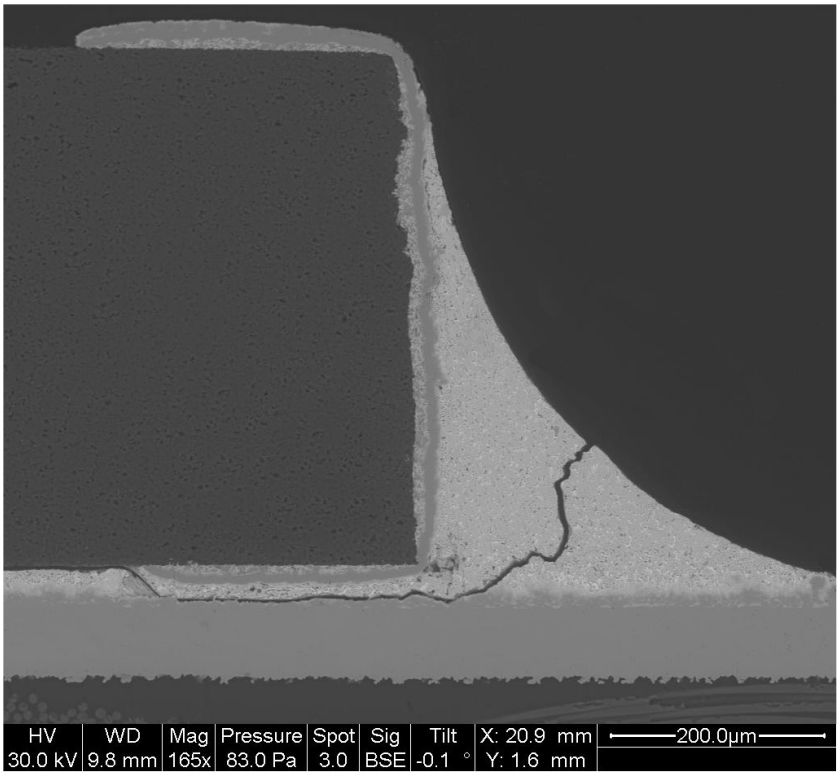

Figure A.2. 5 – Mixed-HASL

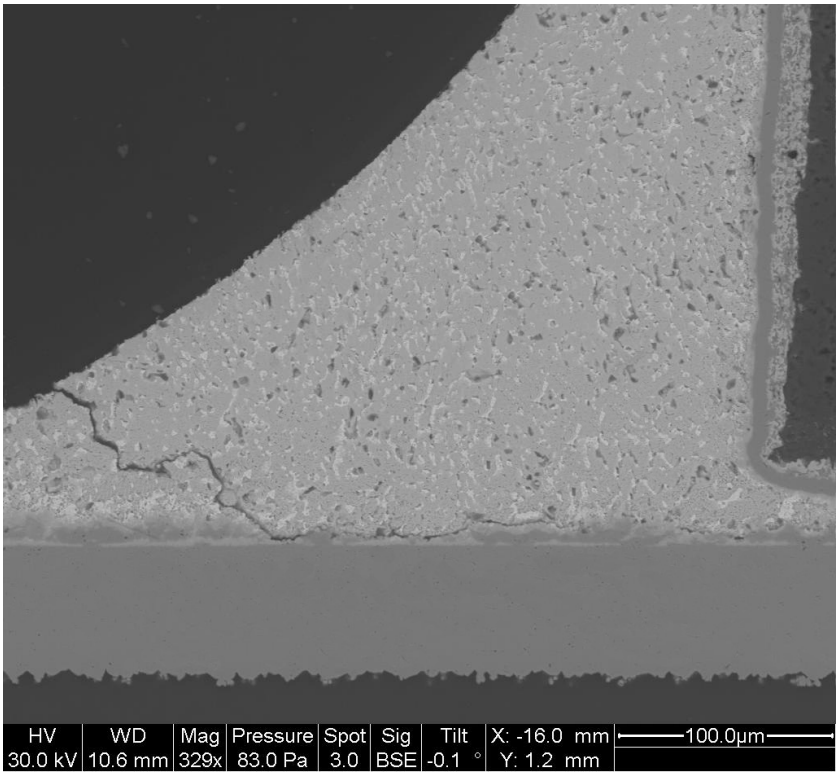

Figure A.2. 6 – Mixed-HASL

A.3 Mixed – ImSn

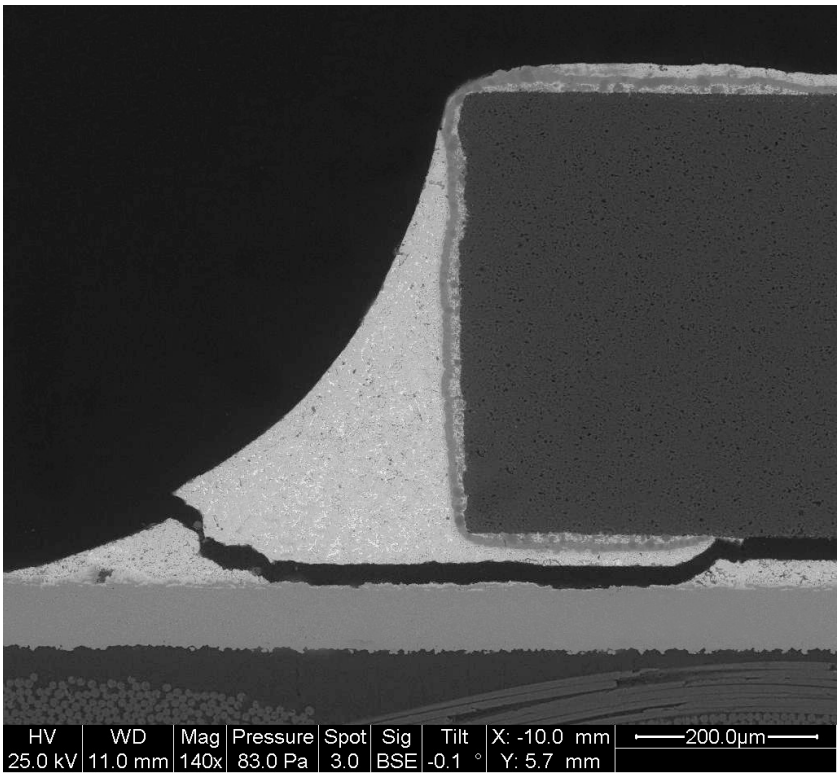

Figure A.3. 1 – Mixed-ImSn

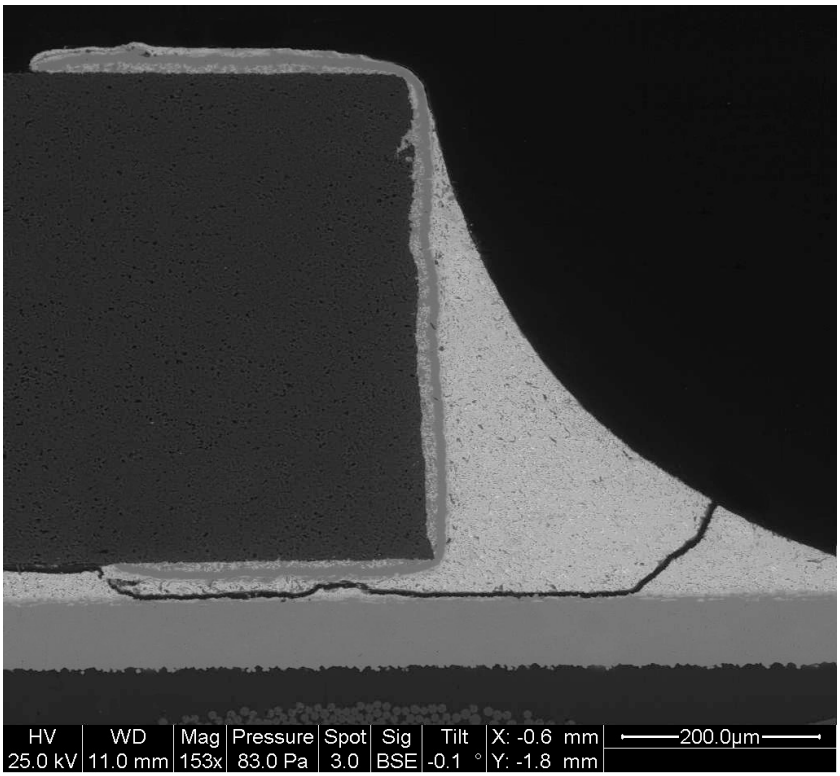

Figure A.3. 2 - Mixed-ImSn

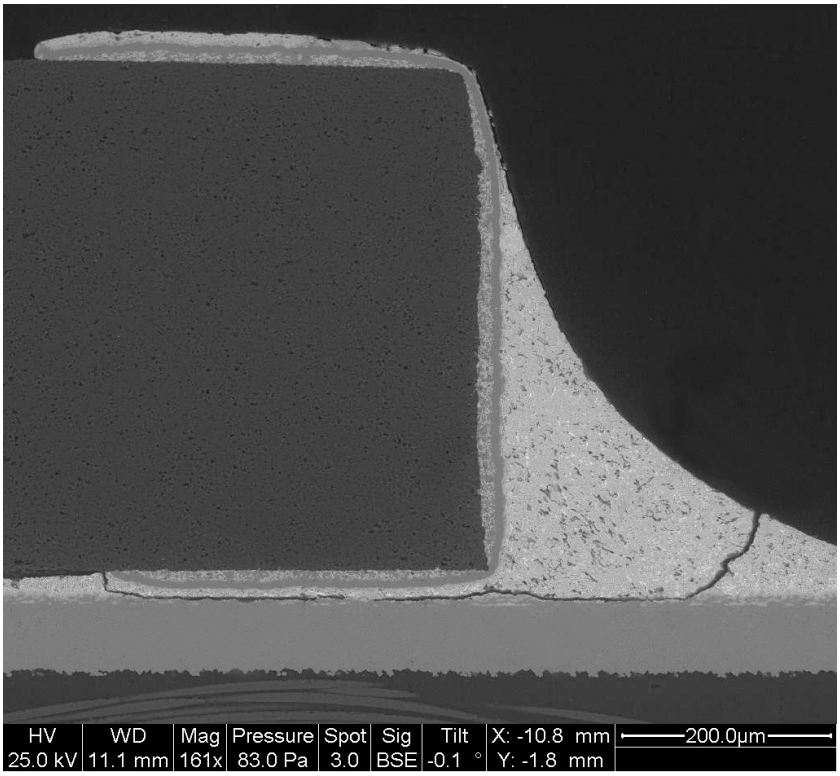

Figure A.3. 3 - Mixed-ImSn

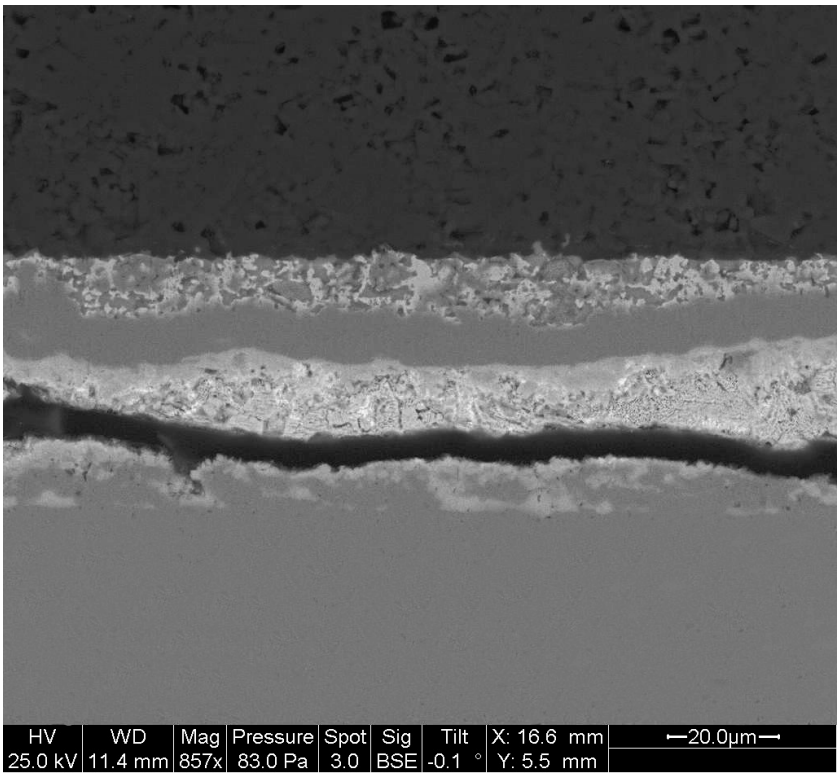

Figure A.3. 4 - Mixed-ImSn

A.4 SAC – ImSn

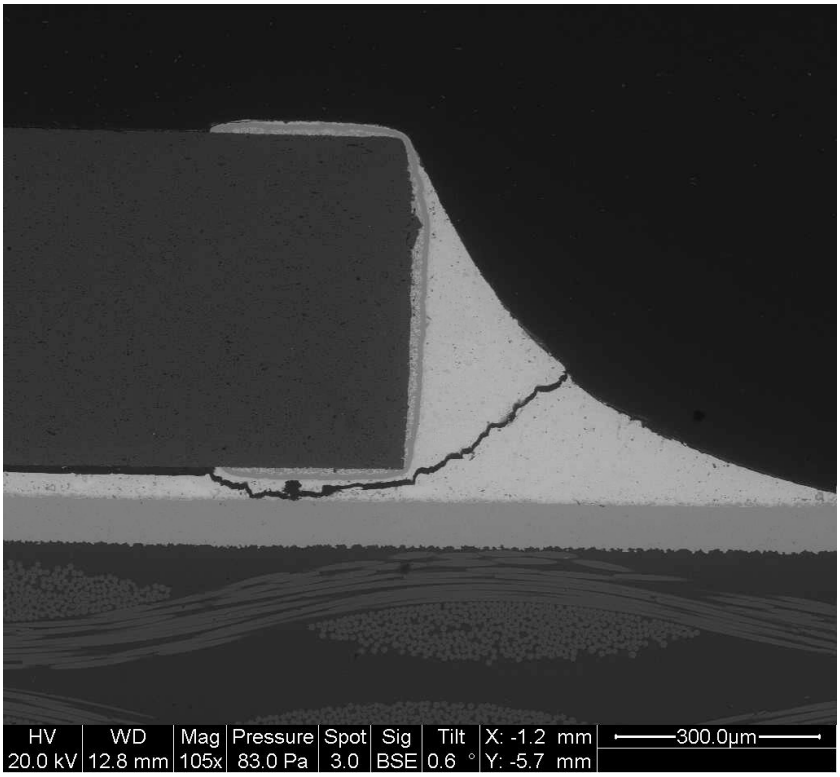

Figure A.4. 1 - SAC-ImSn

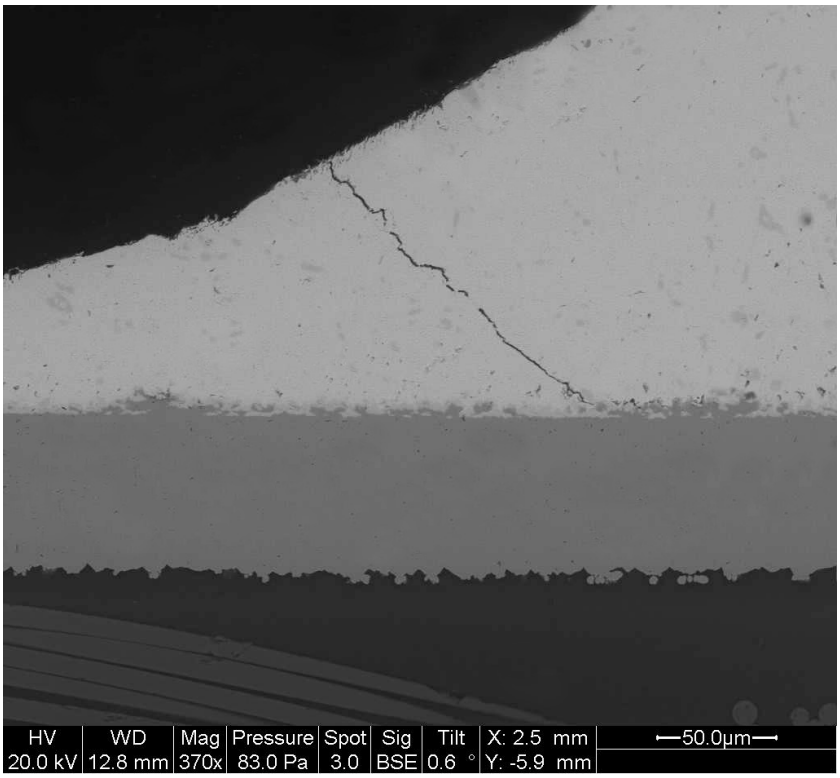

Figure A.4. 2 - SAC-ImSn

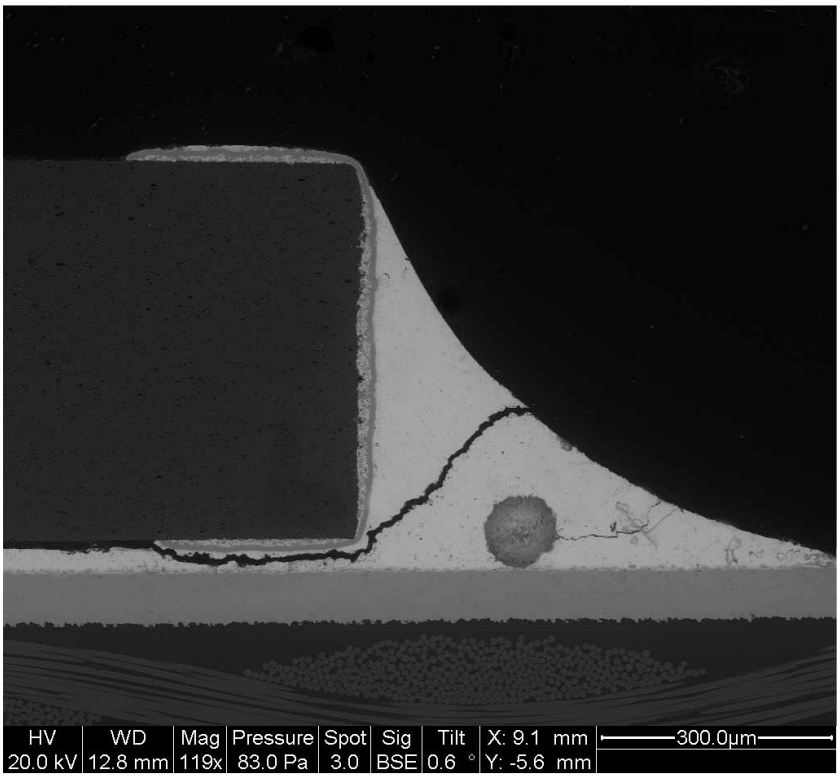

Figure A.4. 3 - SAC-ImSn

A.5 SAC – ImAg

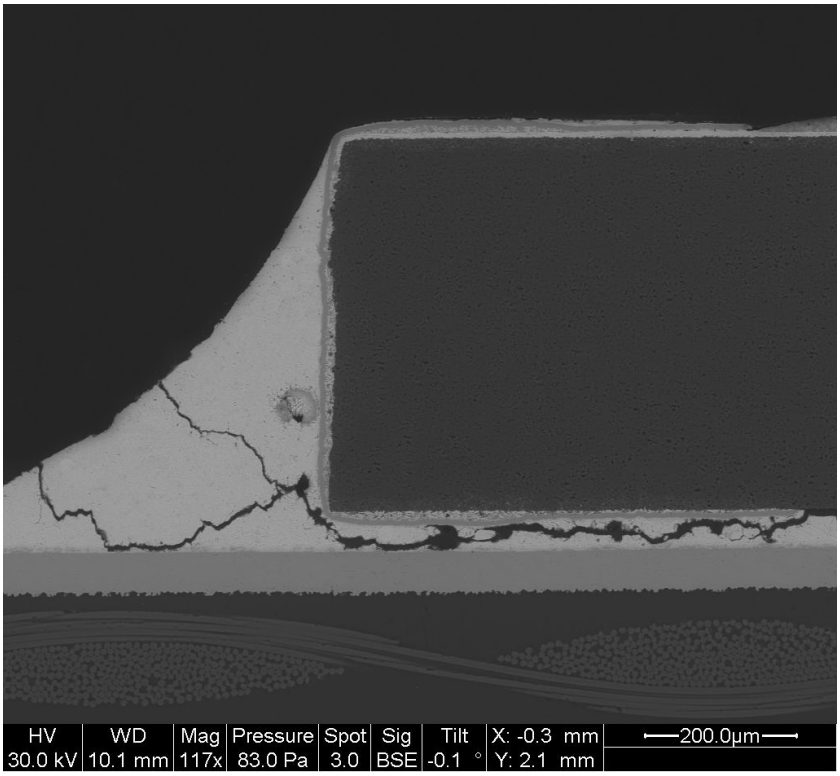

Figure A.5. 1 - SAC-ImAg

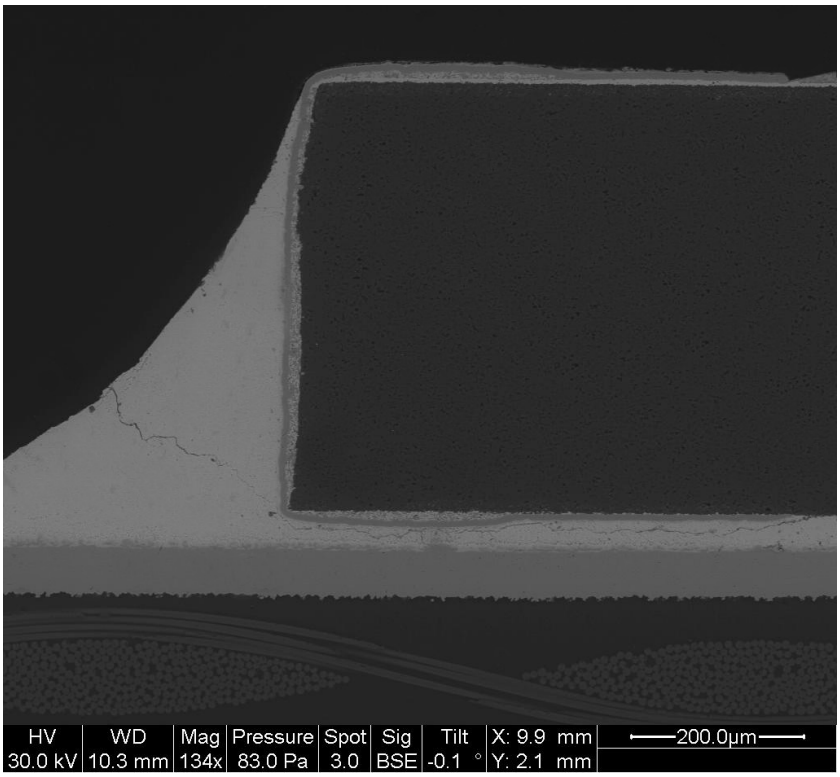

Figure A.5. 2 - SAC-ImAg

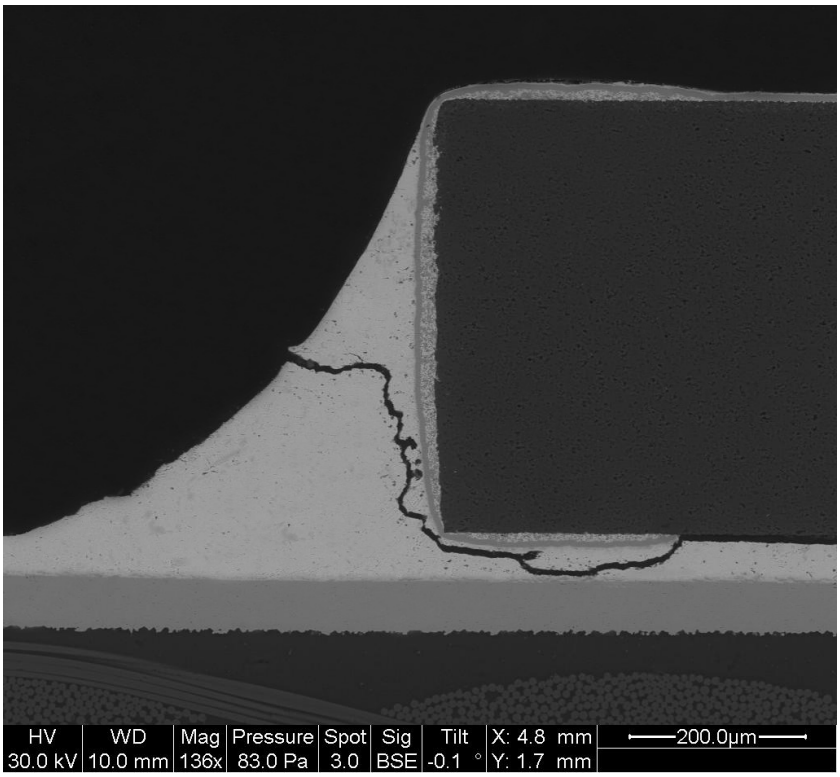

Figure A.5. 3 - SAC-ImAg

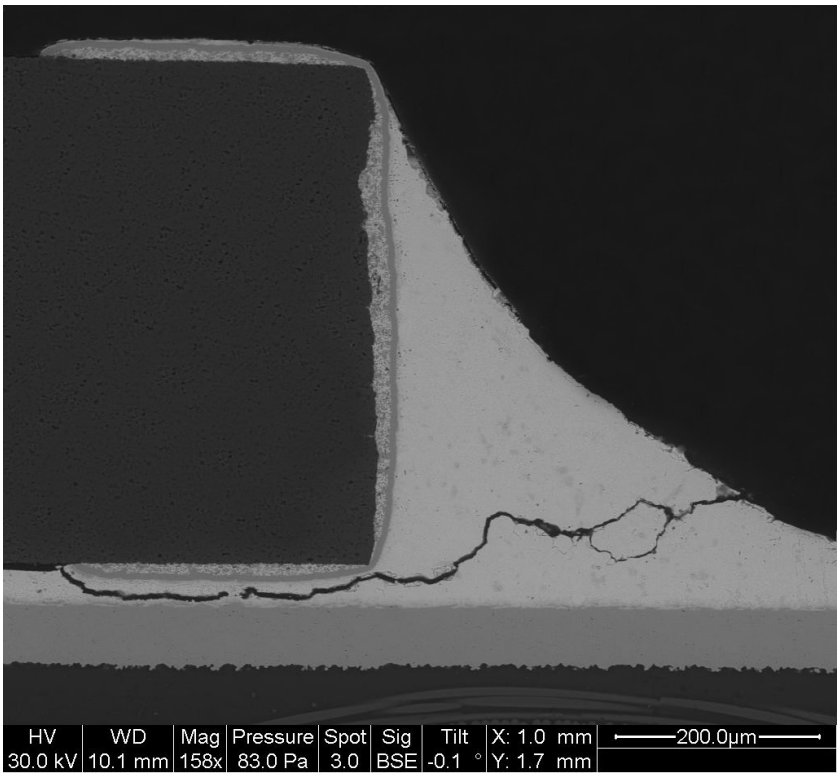

Figure A.5. 4 - SAC-ImAg

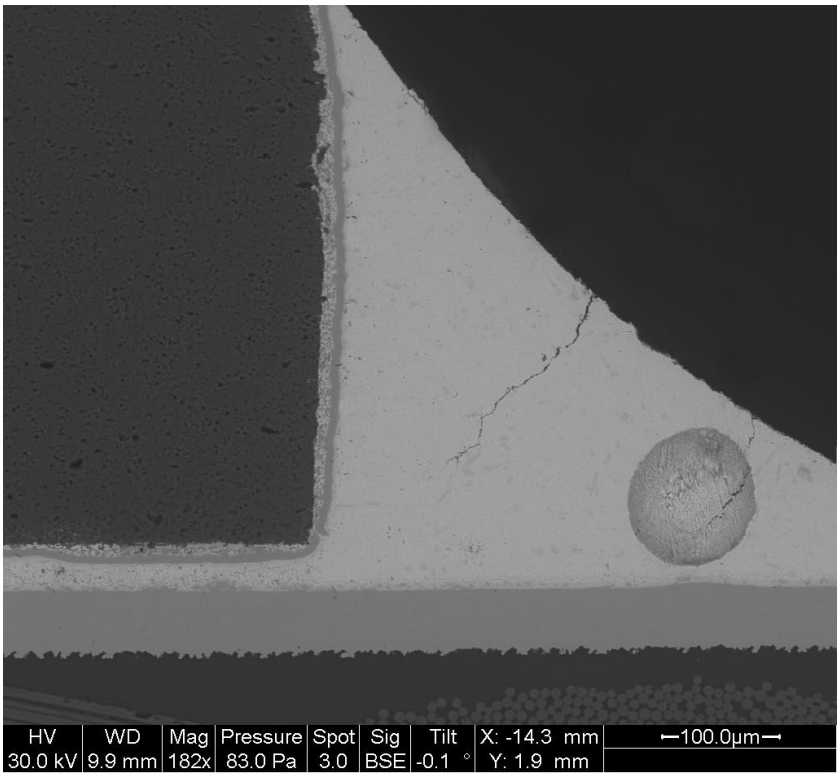

Figure A.5. 5 - SAC-ImAg

A.6 SAC – ENIG

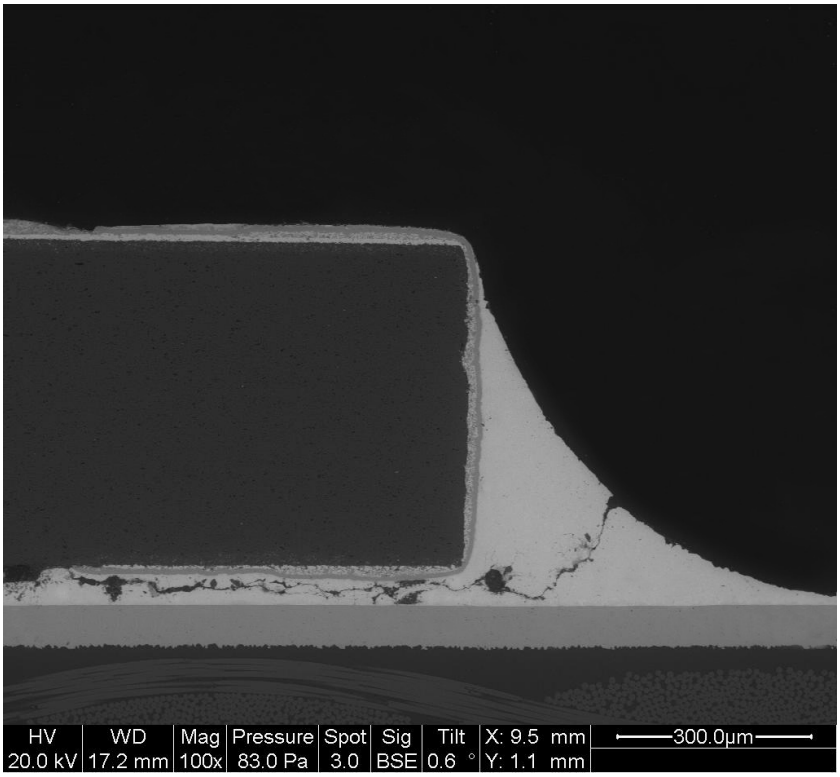

Figure A.6. 1 - SAC-ENIG

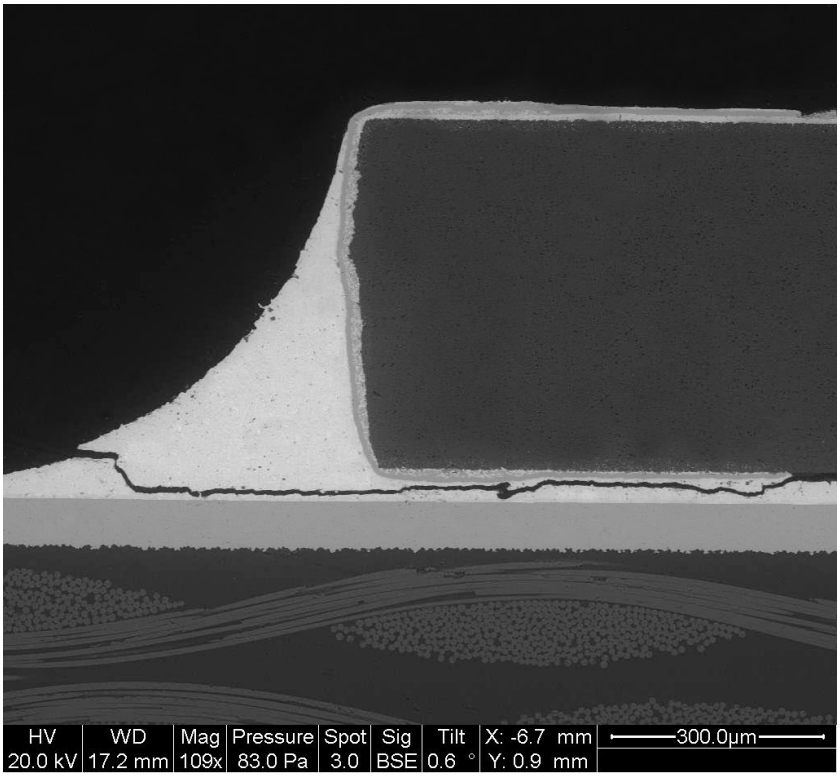

Figure A.6. 2 - SAC-ENIG

A.7 SAC – OSP

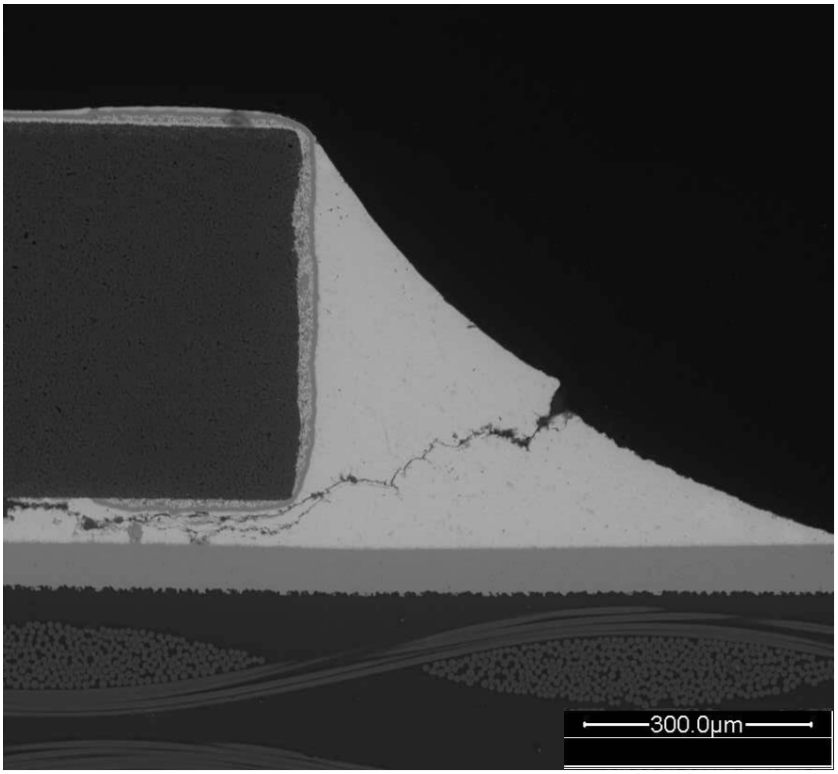

Figure A.7. 1 - SAC-OSP

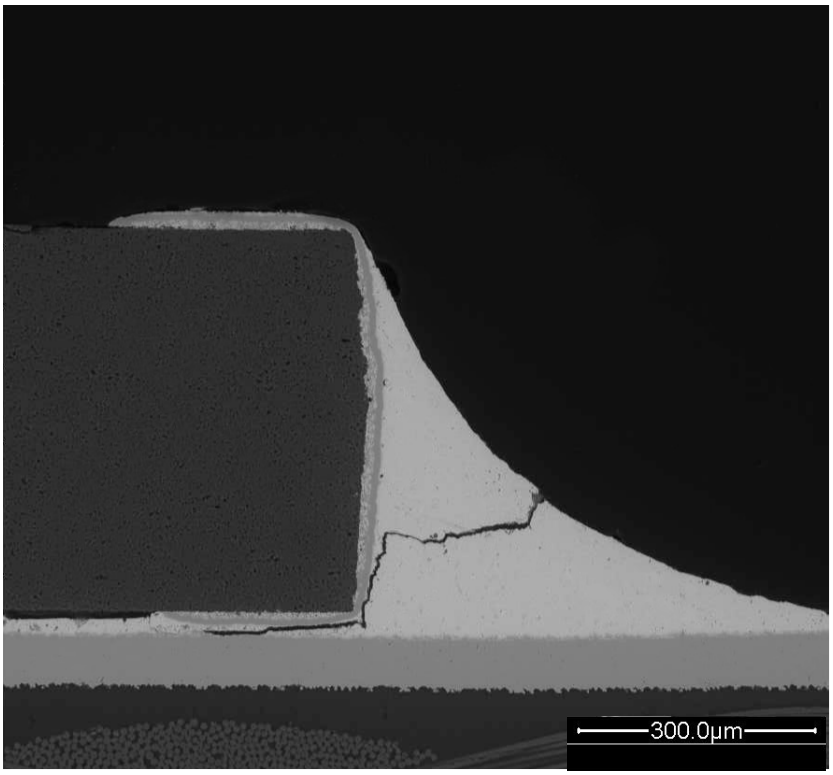

Figure A.7. 2 - SAC-OSP

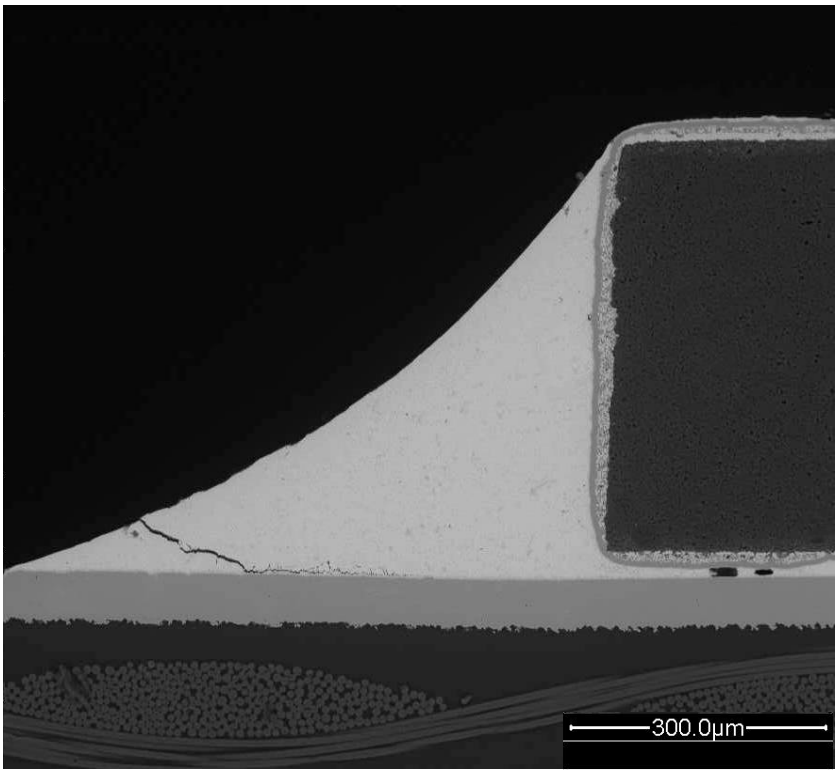

Figure A.7. 3 - SAC-OSP

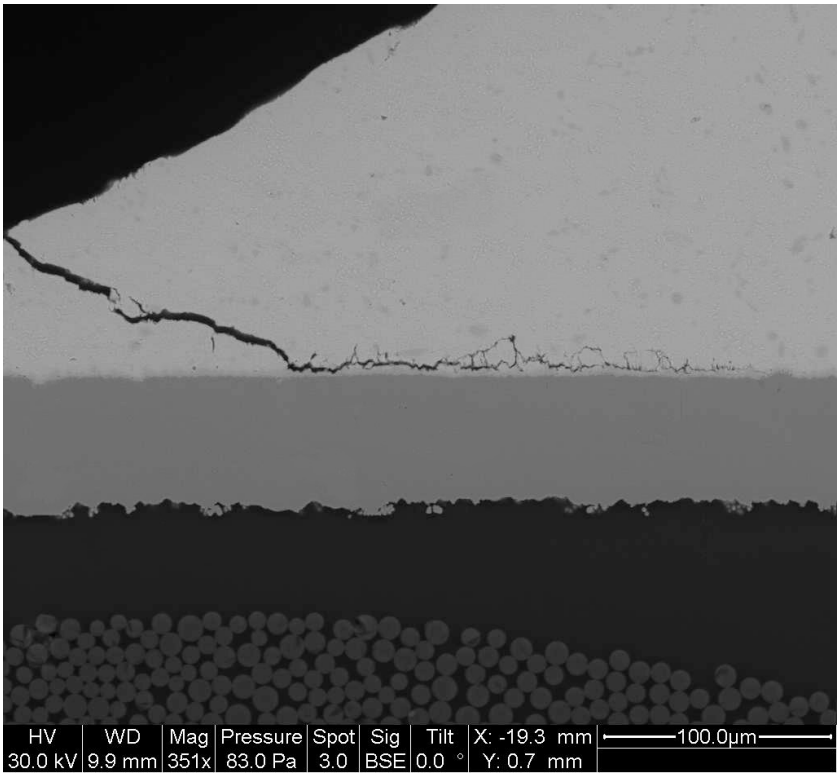

Figure A.7. 4 - SAC-OSP

APPENDIX B – Time to Failure Data (minutes) in Section 3.4

	SnPb - HASL	
	Board 9	**Board 10**
2512 - 3	833	545
2512 - 1	777	728
2512 - 11	1158	801
2512 - 9	831	656

	Mixed - HASL	
	Board 9	**Board 10**
2512 - 3	766	883
2512 - 1	950	1131
2512 - 11	945	907
2512 - 9	1089	988

	SAC-ImSn	
	Board 11	**Board 12**
2512 - 1	1265	446
2512 - 3	887	434
2512 - 11	-	481
2512 - 9	-	608

	Mixed - ImSn	
	Board 11	**Board 12**
2512 - 3	1105	1
2512 - 1	1141	709
2512 - 11	884	597
2512 - 9	992	789

	SAC-ImAg	
	Board 13	**Board 14**
2512 - 1	937	920
2512 - 3	963	899
2512 - 11	890	860
2512 - 9	989	957

	Mixed - ImAg	
	Board 13	**Board 14**
2512 - 3	1023	1090
2512 - 1	928	1139
2512 - 11	1127	1101
2512 - 9	1169	1258

	SAC-ENIG	
	Board 15	**Board 16**
2512 - 1	1000	725
2512 - 3	743	724
2512 - 11	-	720
2512 - 9	813	748

	Mixed - ENIG	
	Board 15	**Board 16**
2512 - 3	1493	1017
2512 - 1	1549	1153
2512 - 11	1332	780
2512 - 9	1567	977

	SAC-OSP	
	Board 17	**Board 18**
2512 - 1	1085	723
2512 - 3	863	726
2512 - 11	1089	745
2512 - 9	1178	1080

	Mixed - OSP	
	Board 17	**Board 18**
2512 - 3	775	728
2512 - 1	1010	802
2512 - 11	967	748
2512 - 9	1043	916

APPENDIX C – TTF Data Adjustment in Section 3.3 and 3.4

In section 3.3, a adjustment procedure was presented to taking into consideration that failures happened within different excitation levels. As a result, a adjustment factor was derived from Steinberg's model and it states:

$$A_{f\,i-j} = \frac{N_i}{N_j} = \left[\frac{\sqrt{PSD_j}}{\sqrt{PSD_i}}\right]^b \qquad \text{Equation 3.7}$$

The adjustment factures that will be used to adjust the failure data are presented in Table 12. The adjusted data from this step is then presented in Table 13, Table 14, and Table 15.

Table 12 – Excitation Level Adjustment Factors

	SnPb	**SAC**
A_f 2-3	9.19	7.73
A_f 2-4	84.45	59.71
A_f 2-1	0.05	0.07

Table 13 – Common Load Level Adjusted SnPb Failure Data (min)

SnPb-HASL
1421
900
10232
1396
204
454
1119
316

Table 14 – Common Load Level Adjusted Mixed Failure Data (min)

Mixed-HASL	Mixed-ImSn	Mixed-ImAg	Mixed-ENIG	Mixed-OSP
797	5799	3166	38586	887
2488	8839	2293	43252	3040
2449	1886	7657	24968	2644
4405	2879	11182	44814	3345
1882	368	4490	3108	453
7973	256	8670	9831	1133
2102	1016	5482	928	639
2844		18719	2739	2183

Table 15 – Common Load Level Adjusted SAC Failure Data (min)

SAC-ImAg	SAC-ImSn	SAC-ENIG	SAC-OSP
2061	14233	2545	3484
2258	1675	562	1697
1695	110	1101	3713
2460	98	419	9028
1928	145	415	416
1765	272	392	436
1463		602	616
2218			3226

After the TTF is adjusted to a single load level, failure data was adjusted to a common frequency response. Equation 3.8 was also derived from Steinberg's empirical model. The results are presented in Table 16, Table 17, and Table 18.

$$N_{normalized} = N_i * \left[\frac{R_{xy} * f_{ni}^{1.25}}{180^{1.25} * R_{xy_i}} \right]^b$$

Equation 3.8

Table 16 – Common Frequency Response Adjusted SnPb Failure Data (min)

SnPb-HASL
1721
1108
12830
1788
431
1023
2712
834

Table 17 – Common Frequency Response Adjusted Mixed Failure Data (min)

Mixed-HASL	Mixed-ImSn	Mixed-ImAg	Mixed-ENIG	Mixed-OSP
1607	11170	5827	323268	2334
5334	18035	4452	446363	8725
5624	4104	15778	327040	8367
10971	6754	24714	783755	11877
2882	714	12343	18959	1140
12672	528	26110	71290	3098
3480	2244	18285	8195	1917
4940		70473	30636	7307

Table 18 – Common Frequency Response Adjusted SAC Failure Data (min)

SAC-ImSn	SAC-ImAg	SAC-ENIG	SAC-OSP
14233	4543	9863	10449
1675	5339	2468	5621
242	4335	6594	13759
232	6900	1256	38197
370	4251	1375	554
762	4173	1452	596
	3742	2546	864
	6221		4669

APPENDIX D – Analysis of the Variance (ANOVA) in Section 3.5

D.1 ANOVA Mixed – Solder Data

SUMMARY

Groups	*Count*	*Sum*	*Average*	*Variance*
Mixed-HASL	8	47511	5938	15182470
Mixed-ImSn	7	43549	6221	41226437
Mixed-ImAg	8	177982	22247	441232655
Mixed-ENIG	8	2009505	251188	7.52E+10
Mixed-OSP	8	44765	5595	15730936

ANOVA

Source of Variation	*SS*	*df*	*MS*	*F*	*P-value*	*F crit*
Between Groups	3.71E+11	4	9.28E+10	5.95	0.001	2.65
Within Groups	5.30E+11	34	1.56E+10			
Total	9.01E+11	38				

D.2 ANOVA SnPb – HASL vs. Mixed – HASL

SUMMARY

Groups	*Count*	*Sum*	*Average*	*Variance*
SnPb-HASL	8	22446	2805	16898297
Mixed-HASL	8	47511	5938	15182470

ANOVA

Source of Variation	*SS*	*df*	*MS*	*F*	*P-value*	*F crit*
Between Groups	39267167	1	39267167	2.45	0.14	4.60
Within Groups	224565370	14	16040384			
Total	263832537	15				

D.3 ANOVA SnPb – HASL vs. Mixed – ImSn

SUMMARY

Groups	*Count*	*Sum*	*Average*	*Variance*
SnPb-HASL	8	22446	2805	16898297
Mixed-ImSn	7	43549	6221	41226437

ANOVA

Source of Variation	*SS*	*df*	*MS*	*F*	*P-value*	*F crit*
Between Groups	43555551	1	43555551	1.55	0.24	4.67
Within Groups	3.66E+08	13	28126669			
Total	4.09E+08	14				

D.2 ANOVA SnPb – HASL vs. Mixed – ImAg

SUMMARY

Groups	*Count*	*Sum*	*Average*	*Variance*
SnPb-HASL	8	22446	2805	16898297
Mixed-ImAg	8	177982	22247	441232655

ANOVA

Source of Variation	*SS*	*df*	*MS*	*F*	*P-value*	*F crit*
Between Groups	1.51E+09	1	1.51E+09	6.60	0.02	4.60
Within Groups	3.21E+09	14	2.29E+06			
Total	4.72E+09	15				

D.2 ANOVA SnPb – HASL vs. Mixed – ENIG

SUMMARY

Groups	*Count*	*Sum*	*Average*	*Variance*
SnPb-HASL	8	22446	2805	16898297
Mixed-ENIG	8	2009506	251188	7.52E+10

ANOVA

Source of Variation	*SS*	*df*	*MS*	*F*	*P-value*	*F crit*
Between Groups	2.47E+11	1	2.47E+11	6.56	0.02	4.60
Within Groups	5.27E+11	14	3.76E+10			
Total	7.74E+11	15				

D.2 ANOVA SnPb – HASL vs. Mixed – OSP

SUMMARY

Groups	*Count*	*Sum*	*Average*	*Variance*
SnPb-HASL	8	22446	2805	16898297
Mixed-OSP	8	44765	5595	15730936

ANOVA

Source of Variation	*SS*	*df*	*MS*	*F*	*P-value*	*F crit*
Between Groups	31133700	1	31133700	1.91	0.19	4.60
Within Groups	228404631	14	16314616			
Total	259538331	15				

D.2 ANOVA SAC Data

SUMMARY

Groups	*Count*	*Sum*	*Average*	*Variance*
SAC ImSn	6	17513	2918	31018795
SAC ImAg	8	39504	4938	1237676
SAC ENIG	7	25554	3650	10937848
SAC OSP	8	74709	9338	1.59E+08

ANOVA

Source of Variation	*SS*	*df*	*MS*	*F*	*P-value*	*F crit*
Between Groups	1.84E+08	3	61385477	1.14	0.35	2.99
Within Groups	1.34E+09	25	53760882			
Total	1.53E+09	28				

D.2 ANOVA SAC vs. SnPb

SUMMARY

Groups	*Count*	*Sum*	*Average*	*Variance*
Column 1	31	158272	5105	21351553
Column 2	29	157282	5423	54577803

ANOVA

Source of Variation	*SS*	*df*	*MS*	*F*	*P-value*	*F crit*
Between Groups	1514893	1	1514893	0.04	0.84	4.01
Within Groups	2.17E+09	58	37391811			
Total	2.17E+09	59				

Bibliography

[1] S. Ganesan and M. Pecht, Lead-Free Electronics. New York: Wiley, 2006.

[2] T. Wong, H. Fenger, "Vibration and Thermo-Mechanical Durability Assessment in Advanced Electronic Package Interconnects", Electronic Components and Technology Conference, Vol. 1, pp. 1080-1087, 1-4 June 2004.

[3] J. Pang, F. Che, and T. Low, "Vibration Fatigue Analysis For FCOB Solder Joints", Electronic Components and Technology Conference, Vol. 1, pp. 1055-1061, 1-4 June 2004.

[4] Y. Chen, C. Wang, and Y. Yang, "Combining Vibration Test with Finite Element Analysis for the Fatigue Life Estimation of PBGA Components", Microelectronics Reliability (2007), doi:10.1016/j.microrel.2007.11.006.

[5] S. Wong, P. Malatkar, C. Rick, V. Kulkarni, and U. Chin, "Vibration Testing and Analysis of Ball Grid Array Package Solder Joint", Electronic Components and Technology Conference, pp. 373-380 May 29-June 1 2007.

[6] Y. Zhou, and A. Dasgupta, "vibration Durability Assessment of Sn3.0Ag0.5Cu and Sn37Pb Solders Under Harmonic Excitation", ASME - IMECE, November 11-16, 2007.

[7] H. Qi, "Plastic Ball Grid Array Solder Joint Reliability Assessment under Combined Thermal Cycling and Vibration Loading Conditions" Ph.D. Thesis, University of Maryland, 2006.

[8] J. Gu, D. Barker and M. Pecht, "Prognostics Implementation for Electronics Under Vibration Loading" Microelectronics Reliability, Vol. 47, Issue 12, pp. 1849-1856, Dec. 2007.

[9] O. H. Basquin, "The Exponential Law of Endurance Tests", *ASTM Proceedings,* vol.10, 1910, pp. 625-630.

[10] D. Steinberg, "Vibration analysis for Electronic Equipment", John Wiley & Son, Third Edition, NY, 2000.

[11] G. Plaza, Y. Zhou, M. Osterman, and A. Dasgupta, "SnAgCu (SAC) Durability Under Vibration Loading at Different Isothermal Temperature Conditions", Proceedings of ASME Interpack 2007, Paper No. IPACK2007-33095, 2007.

[12] T. Woodrow, "JCAA/JG-PP Lead-free Solder Project: Vibration Test", SMTA International, 2005.

[13] T. Woodrow, "JCAA/JG-PP Lead-free Solder Project: Vibration Test", Boeing Electronics Materials and Processes Report – 582, Revision A, 2006.

[14] Lee, R. Lui, W., "Evaluation of Board Level Reliability of Pb-free PBGA Solder Joints", IEEE Transactions on Advanced Packaging Materials, pp. 82-89, 2002.

[15] N. Barry, I Jones, T Hirst, I. Fox, J. Robins, "High-cycle Fatigue Testing on Pb-free Solder Joints", Soldering & Surface Mount Technology, Vol. 19, pp. 29-38, 2007.

[16] United States Environmental Protection Agency, "Alternative Technologies for Surface Finishing: Clear Technologies for Printed Wiring Board Manufacturers", Technical Report, EPA-744-R-01-001, pp. 1-42, 2001.

[17] P. Vianco, "An Overview of Surface Finishes and Their Role in Printed Circuit Board Solderability and Solder Joint Performance", Circuit World, Vol. 25, No. 1, pp. 6-24, 1998.

[18] A. Spowage, C. Thong, and P Collier, " Effect of Surface Finishes on the Thickness and Morphology of the Intermetallic Layer in Lead-Free Solder Joints", International Journal of Nanoscience, Vol. 3, No. 6, pp. 803-813, 2004.

[19] K. Zeng, and K. Tu, "Six Cases of Reliability Study of Pb-free Solder Joints in Electronic Packaging Technology", Materials Science and Engineering R, Vol. 38, pp. 55-105, 2002.

[20] D. Goyal, T. Lane, P. Kinzie, C. Panichas, K. Chong, and O. Villalobos, "Failure Mechanism of Brittle Solder Joint Fracture in the Presence of Electroless Nickel Immersion Gold (ENIG) Interface", Electronic Components and Technology Conference, pp. 732-739, 2007.

[21] J. Fang, and D. Chan, "The Advantages of Mildly Alkaline Immersion Silver as a Final Finish for Solderability", Circuit World, Vol 33, No. 2, pp. 43-51, 2007.

[22] T. Graedel, "Corrosion Mechanisms for Silver Exposed to the Atmosphere", Journal of Electrochemical Society, Vol. 139, No. 7, pp. 1963-1970, 1992.

[23] F. D. Houghton, "Alternative Metallic Surface Finishes an Update on the ITRI/October Project," Proceedings of the IPC Printed Circuits Expo 1998, Paper no. S14-6, April 26-30, 1998.

[24] H. Qi, S. Ganesan, J. Wu, M. Pecht, P. Matkowski, and J. Felba, "Effects Printed Circuit Board Materials on Lead-free Interconnect Durability", 5th International Conference on Polymers and Adhesives in Microelectronics and Photonics, pp. 140-144, Wroclaw, Poland, October 23-26, 2005.

[25] Standard IPC-SM-785, "Guidelines for Accelerated Reliability Testing of Surface Mount Solder Attachments," The Institute for Interconnecting and Packaging Electronic Circuits, Northbrook, IL, November 1992.

[26] Standard IPC-9701, “Test Methods and Qualification Requirements for Surface Mount Solder Attachments” The Institute for Interconnecting and Packaging Electronic Circuits, Northbrook, IL, January 2002.

[27] N. Blattau and C. Hillman, “A Comparison on the Isothermal Fatigue Behavior of SnAgCu to SnPb Solder”, Surface Mount Technology Association International Conference, Chicago, IL, September 29, 2005.

[28] CALCE_PWA, Version 4.1, User Manual, University of Maryland-College.